



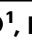


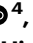







Stimulation of corticospinal neurons by optogenetic cAMP inductions promotes motor recovery after spinal cord injury in female rats via raphespinal tract modulation

Received: 24 November 2024

Accepted: 11 June 2025

Published online: 01 July 2025

 Check for updates

Beatriz Martínez-Rojas ^{1,9} , Samuel Martín-Pérez ¹, Esther Giraldo ^{1,2,3}, Eric Lopez-Mocholi ¹, Ana Alastrue¹, Yuniesky Andrade-Talavera ⁴, Jose Prius-Mengual⁴, Guillem Paniagua ¹, Maria Pedraza^{1,5}, Sonia Hingorani¹, Benjamin R. Rost ⁶, Dietmar Schmitz^{6,7}, Marta Llansola ⁸, Vicente Felipo ⁸, Antonio Rodríguez-Moreno ⁴ & Victoria Moreno-Manzano ^{1,2,9} 

After spinal cord injury (SCI), cyclic adenosine monophosphate (cAMP) levels drop in the spinal cord, cortex and brainstem, unlike in regenerating peripheral neurons. To address SCI recovery, we expressed photoactivatable adenylate cyclase (bPAC) in corticospinal neurons of female rats with dorsal hemisection for on-demand cAMP inductions. bPAC stimulation restored passive and firing properties of corticospinal neurons, promoted early and sustained locomotor recovery and increased corticospinal tract plasticity. Additionally, bPAC enhanced sparing of lumbar-projecting brainstem neurons after SCI, accompanied by activation of cAMP signaling in the raphe-reticular formation and increased excitatory/inhibitory neurotransmitter balance. Accordingly, augmented density of serotonergic tracts was found caudal to the injury in bPAC rats, correlating with enhanced functional performance. Serotonergic implication in motor recovery was further evidenced by selective depletion, resulting in the abrogation of bPAC-mediated recovery. Overall, our findings underscore that cAMP induction in corticospinal neurons enhances locomotion after SCI, through a cortical rerouting pathway via the serotonergic descending tract.

During walking, the brain sends executive commands to the spinal cord through descending tracts, forming synapses with interneurons or motor neurons that engage the target muscle¹. Spinal cord injury (SCI) disrupts the sophisticated array of connections, depriving lower spinal neurons of supraspinal inputs that,

ultimately, render them non-functional² resulting in dramatic locomotor deficits³.

The corticospinal tract (CST) represents the most relevant supraspinal pathway for skilled voluntary motor control in humans, especially finger dexterity⁴. CST originates from pyramidal neurons

¹Neuronal and Tissue Regeneration Laboratory, Centro de Investigación Príncipe Felipe, Valencia, Spain. ²Department of Biotechnology, Universitat Politècnica de València, Valencia, Spain. ³UPV-CIPF Joint Research Unit Disease Mechanisms and Nanomedicine, Centro de Investigación Príncipe Felipe, Valencia, Spain. ⁴Laboratory of Cellular Neuroscience and Plasticity, Department of Physiology, Anatomy and Cell Biology, University Pablo de Olavide, Seville, Spain. ⁵Sharestist, Valencia, Spain. ⁶German Center for Neurodegenerative Diseases (DZNE), Berlin, Germany. ⁷Institute of Cell Biology and Neurobiology & Neuroscience Research Center, Charité Universitätsmedizin Berlin, Berlin, Germany. ⁸Laboratory of Neurobiology, Centro de Investigación Príncipe Felipe, Valencia, Spain. ⁹These authors jointly supervised this work: Beatriz Martínez-Rojas, Victoria Moreno-Manzano. ✉ e-mail: bmartinezrojas@outlook.es; vmorenom@cipf.es

of the layer V that project to the dorsal (95%) or the ventral and lateral funiculus (5%) of the spinal cord^{5,6}. Additionally, other phylogenetically older motor centers also directly connect with the spinal cord⁷. Within the brainstem, neurons located in the gigantocellular nucleus (Gi), the lateral paragigantocellular nucleus (LPGi), and the ventral gigantocellular nucleus (VGI or GiA) of the reticular formation give rise to the reticulospinal tract (RtST), which descends through the ventral and lateral funiculi of the spinal cord^{8–10}. In close anatomic proximity, the serotonergic tract (the major component of the raphespinal tract, RpST) arises from serotonergic cells distributed in the caudal raphe nuclei, including the raphe magnus, pallidus, and obscurus but also scattered throughout the reticular formation¹¹. Notably, neurons of Layer V of the motor cortex send cortico-bulbar projections to the brainstem, delineating an alternative indirect pathway to the spinal cord^{12,13}.

The CST is especially reluctant to axonal regeneration^{14,15} after SCI. Promising preclinical therapies have achieved varying degrees of CST axonal outgrowth into the injury site^{16–19}; however, long-distance CST elongation still remains inconceivable. New evidence recently suggested that CST sparing below the injury level is not strictly required to recover cortical control over leg motor neurons²⁰. CST regeneration across the injury represents only one means for cortical commands to reach sublesional areas after SCI²⁰. Supralesional CST sprouting to contact propriospinal neurons²¹ or cortico-brainstem rewiring²² represent validated mechanisms to reroute the cortical networks to bypass the injury. Thus, the field recently faced a new paradigm shift towards therapies focused on exploiting the potential of spared tracts, leaving behind the conventional focus on injury containment, cell replacement, or damaged fiber regeneration. Excitingly, neuromodulatory therapies have already seen successful translation into human patients^{23,24}.

In the present study, we explored the therapeutic potential of neuromodulation of corticospinal neurons by daily cyclic adenosine monophosphate (cAMP) elevations after SCI. Our therapeutic approach takes inspiration in the conditioning lesion paradigm in dorsal root ganglion (DRG) neurons where cAMP levels are tripled one day after peripheral axon injury, which induces a state of regenerative competence to the spinal central branch when consecutively injured^{25,26}. Moreover, cAMP analog (db-cAMP) injections into the DRG before SCI completely mimic the conditioning lesion effect promoting dorsal column axon regeneration. These findings suggest that cAMP increases after the conditioning lesion are responsible for the acquisition of a growth-competent state²⁶. However, cAMP fails to increase in neurons after CNS injury; instead, cAMP levels sustainably drop in the spinal cord (64.3%), sensorimotor cortex (69.7%), and brainstem (68.1%) within one-day post-SCI²⁷. Thus, we propose ectopic cAMP induction in corticospinal neurons to mimic the conditioning lesion effect and trigger regeneration after SCI.

The photoactivatable adenylate cyclase extracted from the soil bacterium *Beggiatoa* (bPAC) is a homodimeric protein containing a BLUF domain, which displays sensitivity to blue light stimulation, linked to an adenylate cyclase domain. bPAC serves as an optogenetic tool suitable for on-demand cAMP increases in living animals, enabling cell-specific expression when controlled under specific promoters and through localized injection of adeno-associated viral constructs, thereby minimizing undesirable off-target effects²⁸. Xiao et al. previously applied bPAC in afferent neurons in a Zebrafish spinal cord injury model, reporting significantly enhanced axonal regeneration following axotomy and reinnervation of their original target area, upon bPAC stimulation²⁹.

Thus, we hypothesized that cAMP stimulation in corticospinal neurons would trigger neuroplastic changes of the CST, ultimately leading to improvements in locomotor function in a rodent model of severe SCI. Overall, our study revealed the effectiveness of inducing cAMP in corticospinal neurons for the purpose of restoring locomotor

function after SCI through a mechanism involving the serotonergic descending pathway.

Results

bPAC stimulation resulted in increased P-CREB and c-Fos levels in the motor cortex of rats with SCI

In vitro evaluation in cultured cortical neurons transduced with either CAMKII-bPAC-mCherry (bPAC) or CAMKII-mCherry (Control) demonstrated that bPAC activation by saturating blue light exposure (480 nm, 90 s, 20 mW/cm²)³⁰ (Fig. 1A) successfully prompted a ≈ 14 -fold increase of cAMP levels (Fig. 1B). Moreover, real-time calcium assays, performed using Fluo-4AM probe, showed that bPAC expressing cortical neurons efficiently increased their intracellular calcium content after blue light stimulation (Fig. 1C and D), possibly through cAMP-gated calcium channel^{31,32}. These results demonstrate that bPAC system is efficient to induce cAMP levels in cortical neurons and that it can additionally prompt intracellular calcium oscillations which may lead to calcium-downstream signaling.

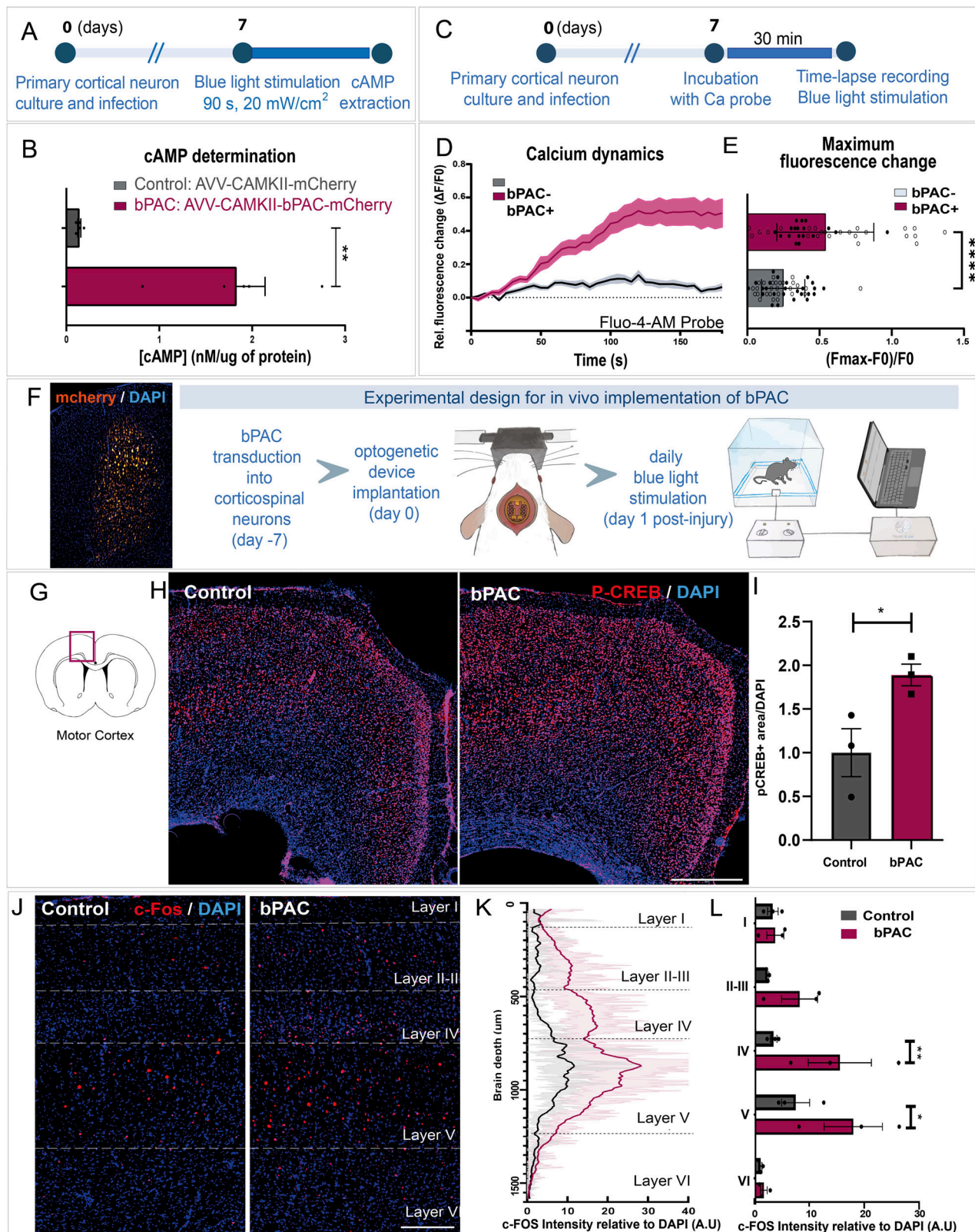
For bPAC expression in rats, AAV2/9-CAMKII-bPAC-mCherry viral particles were stereotactically injected in layer V of the motor cortex. Control animals were likewise injected with AAV1-CAMKII-mCherry or AAV2/9-CAMKII- Δ bPAC-mCherry, as indicated. One week after, time to allow the bPAC protein expression, a spinal cord dorsal hemisection at the 8th thoracic (T8) spinal segment was performed, and a wireless device for time and dose-controlled blue-light stimulation was implanted (Fig. 1F). Ten days after optogenetic stimulation (30 min/day, 1 s ON - 4 s OFF, starting one day after SCI) bPAC rats presented widespread CREB phosphorylation (P-CREB) within the primary motor cortex, as expected after cAMP elevation³³ (Fig. 1G–I), indicative of the suitability of bPAC optogenetic set up for inducing cAMP signaling in vivo. cAMP induction has been previously related to increased neuronal activation, with studies reporting transient neuronal hyperactivation after bPAC-mediated cAMP elevation in the CA1 region of the hippocampus³⁴. In agreement, we detected a significant increase in c-Fos expression after bPAC stimulation, mostly in layers IV and V of the motor cortex (Fig. 1J–L). Neither P-CREB nor c-Fos staining were confined to bPAC-expressing neurons (Supplementary Fig. 1), but rather, these increases were also observed in neighboring neurons, indicating a more widespread activation beyond the bPAC-expressing cells.

Moreover, HPLC quantification of cAMP levels after 10 days of optogenetic stimulation across various regions of the central nervous system revealed a general increase in cAMP levels (Supplementary Fig. 2A). This effect reached statistical significance at the spinal cord segment rostral to the injury site, where cAMP concentrations increased from 4.1 ± 0.62 to $12.2 \pm 0.6 \mu\text{M/mg}$ of tissue in Control vs. bPAC groups, respectively ($p = 0.0001$, one-tailed t-test). The observed accumulation of cAMP in the spinal segment rostral to the injury may reflect the anterograde diffusion of the second messenger along the descending corticospinal axons following cortical stimulation, potentially leading to the formation of cAMP-enriched subdomains at the axonal tips.

Overall, these results demonstrate that daily bPAC stimulation of corticospinal neurons in SCI rats activates cAMP-dependent signaling pathways, as evidenced by increased CREB phosphorylation and c-Fos-associated neuronal activation in the motor cortex, along with elevated cAMP levels at key regions of the central nervous system.

bPAC treatment affects passive electrophysiological properties, increases the excitability of Layer V motor cortex neurons and improves their responsiveness

Ex vivo current-clamp on corticospinal neurons from prefrontal cortex slices ten days after optogenetic stimulation revealed that bPAC-treated group is more prone to spontaneous firing at resting membrane potential (basal, Vm) compared to uninjured and Control



(injured) groups (Fig. 2A). In addition, neurons from bPAC-treated rats showed more depolarized Vm compared with uninjured and Control groups (Fig. 2A, B). Control injured neurons showed increased membrane capacitance (Cm, Fig. 2C) which might be related to the reduced membrane resistance (Rm, Fig. 2D) despite the membrane time constant (τ) not being altered (Fig. 2E). In turn, bPAC treatment restored the parameters that were altered in the Control injured group

(Fig. 2C, D). No significant differences between conditions were found in the passive electrophysiological membrane properties of astrocytes (Supplementary Fig. 3A–D). These results indicate that bPAC treatment affects passive membrane electrophysiological properties of Layer V neurons from the motor cortex and increases their excitability.

To further test whether the bPAC treatment increases the excitability of pyramidal neurons from rats' motor cortex, we applied hyper

Fig. 1 | bPAC stimulation induces cAMP levels and calcium mobilization in primary cortical cultures and increases P-CREB and c-Fos levels in the motor cortex of SCI rats. **A** Experimental design for the in vitro determination of cAMP after saturating blue light exposure (90 s, 20 mW/cm²) in primary cortical neurons. **B** cAMP levels measured by high-performance liquid-chromatography in Control (gray) or bPAC (magenta) cultured cortical neurons normalized to total protein content. Three independent experiments, 2 technical replicates per experiment; $p = 0.0054$. **C** Experimental design for live calcium in vitro assays during blue light stimulation in bPAC-expressing (bPAC+) or non-bPAC expressing (bPAC-) neurons in the same well. **D** Graphs for the change in fluorescent given by Fluo-4AM (green) defined as $Fx-F0/F0$ as well as **(E)** the maximum fluorescent change calculated as $F_{max}-F0/F0$ for each neuron in bPAC+ (magenta) and bPAC- neurons (gray). Sample size reflects individual neurons across two independent experimental replicates; $p < 0.0001$. **F** Experimental schema describing the in vivo

implementation of bPAC strategy. **G** Schema illustrating the brain region analyzed in P-CREB and c-Fos quantifications. **H** Representative images for P-CREB immunolabelling in Control (right) and bPAC (left) injured animals, 10 days after dorsal hemisection and optogenetic stimulation. Scale bar: 500 μ m. **I** Bar-graph for the quantification of the effect of bPAC stimulation on CREB phosphorylation in the motor cortex. Three animals/group, mean of two hemispheres/animal; $p = 0.0207$. **J** Representative images for c-Fos immunostaining, Scale bar: 200 μ m, and **K, L** quantification of the effect of bPAC on c-Fos activation across cortical layers. Three animals/group, mean of 3–5 hemispheres/animal; $p = 0.038$ for the layer V. Data is presented as a mean \pm SEM with statistical significance set as * $p < 0.05$, ** $p < 0.01$, and *** $p < 0.001$ for comparisons using two-tailed unpaired t test (**B**), two-tailed Mann-Whitney test (**E**), Two-way Anova (**L**) and one-tailed t-test (**I**). Source data are provided as a Source Data file.

– and depolarizing pulses (–100 and 250 pA, respectively) during 500 ms. We observed the typical behavior of motor cortex pyramidal neurons^{35,36}. Strikingly, the depolarizing pulse elicited a higher firing rate in the bPAC-treated group than in Control (injured) rats, resulting in a similar pattern to the uninjured condition (Fig. 2F–H). Moreover, the application of multistep depolarizing protocol (10 pA increasing, 700 ms, Fig. 2G) revealed that neurons from bPAC-treated rats possess a more hyperpolarized AP firing threshold (Fig. 2I), with a lower threshold current (Fig. 2J) and lower AP delay at rheobase (Fig. 2K) compared with neurons from Control injured rats. Interestingly, bPAC treatment restores the firing threshold and AP firing delay at the uninjured group levels (Fig. 2I–K). Input-output curve (injected current–Vm changes) showed that neurons from all groups respond similarly (Fig. 2L). However, bPAC-treated rats respond to increasing current intensity with larger Vm variations at very low current intensities (ex., at 20 and 50 pA). More pronounced differences were observed in terms of AP firing rates in response to increasing current intensity (Fig. 2M). In line with the observed lower threshold current at rheobase, neurons from the bPAC-treated group started firing at lower current intensities compared with Control and uninjured groups, reaching a plateau with a significantly larger firing rate. Likewise, the Control group did not reach the firing rate of bPAC and uninjured groups in response to 190 pA intensity. Moreover, bPAC treatment led to firing responses similar to the uninjured group at 190 pA, recovering such firing ability (Fig. 2M). Additional statistical data are available in Supplementary Table 1.

To investigate the excitatory drive onto pyramidal motor cortex neurons, we recorded spontaneous excitatory postsynaptic currents at –70 mV holding Vm. We observed that bPAC treatment provokes a decrease in EPSC amplitude and an increase in the frequency. Thus, bPAC treatment also changes excitatory synaptic transmission at Layer V motor cortex (Supplementary Fig. 3E–G).

Altogether these findings indicate that bPAC treatment affects passive membrane properties, increases the excitability of Layer V motor cortex neurons, and widens their ability to respond to depolarizing inputs. Thus, bPAC treatment recovers the passive and firing properties of Layer V motor neurons from the injured phenotype.

bPAC stimulation in corticospinal neurons improved locomotor recovery after SCI

Next, we explored whether the cAMP-dependent motor cortex activation could drive skilled locomotor improvements after thoracic dorsal hemisection. For that, we evaluated the progressive skilled locomotor recovery in optogenetically stimulated rats (bPAC) or Control for 35 days after SCI (Fig. 3A–F). Post-mortem evaluation of the injury via the histological study of GFAP-negative and cyst-filled areas confirmed no differences in the injury size (GFAP negative staining) nor the Neun gap across the injury between Control and bPAC rats (Fig. 3B), demonstrating the consistency of injuries between the two experimental groups.

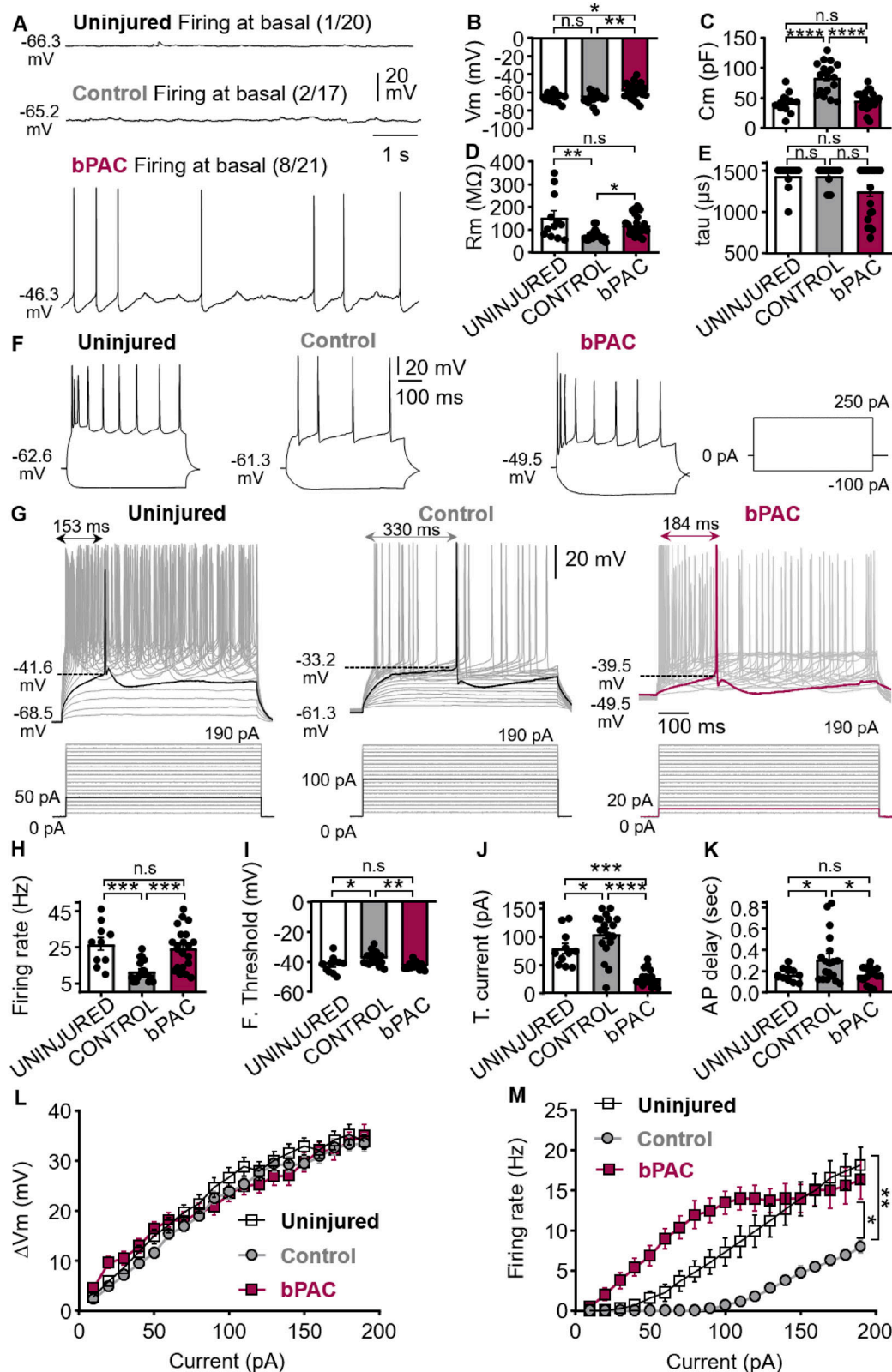
While all animals gradually recovered a certain degree of motor function during the period under study; bPAC animals achieved higher Basso, Beattie, and Bresnahan (BBB) scores, significantly different at day 6 and 10 post-injury, and then sustained over the entire 35-day period (Fig. 3C). Specifically, bPAC rats elicited a pronounced early recovery compared to Control; by day 10 after injury 100% of bPAC rats had recovered the ability to support their weight with hind paws and perform frequent plantar stepping (BBB score ≥ 11), while only 55.5% of the Control rats exhibited weight-bearing capacity at that time. This result was validated by the measurement of the height of the iliac crest during walking (Fig. 3D).

We further interrogated more skilled locomotion once the animals had recovered their weight support capacity by evaluating their scores when crossing through a horizontal ladder or narrow beam. Those tests are useful for easily discerning animals with more consistent forelimb-to-hindlimb coordination and balanced stepping, allowing the discrimination between an individual with the same score in open-field testing³⁷. bPAC rats outperformed Controls throughout the time period under study in both tests (Fig. 3E) being the differences statistically significant on day 6 and 10 for ladder beam and day 17, 29 and 35 for narrow beam. Finally, to evaluate finer locomotion, at the endpoint (day 35), we assessed hind-limb joint kinematics using TSE Motorater system³⁸. bPAC rats exhibited hip, knee, and ankle angle range curves during the step cycle more similar to uninjured animals than Control (injured) animals (Fig. 3F). All the collected locomotor parameters were integrated in a principal component analysis revealing a clear segregation between bPAC and Control rats, which provides robust evidence of bPAC's efficacy in promoting a differential locomotor recovery (Fig. 3G).

Additionally, we studied thermal hyperalgesia (as an indicator of neuropathic pain) by the thermal test of hind limb paws (Fig. 3H). Our result displayed no significant difference between Control and bPAC rats, demonstrating the absence of unintended effects on nociceptive perception.

This functional data demonstrates that cAMP induction by daily optogenetic bPAC stimulation in the corticospinal neurons results in early locomotor recovery and improves fine locomotor skills without affecting nociception after severe dorsal thoracic SCI.

Histological analysis of the CST using anterograde labeling with AAV2/9-CaMKII-bPAC-mCherry (bPAC) or the inactive mutant construct AAV2/9-CaMKII- Δ bPAC-mCherry (Control)³⁹, revealed increased mCherry+ area in the spinal segment rostral to the injury in bPAC group compared to controls ($p = 0.008$, $n = 4$ per group) (Fig. 3I–J). A similar trend was observed caudal to the lesion, although it did not reach statistical significance. This finding may suggest enhanced CST sprouting into the surrounding gray matter in response to bPAC stimulation, resulting in an expanded distribution of labeled and fibers innervating the intermediate and ventral neurons.



bPAC stimulation improves the preservation/regeneration of descending tracts from Layer V of the motor cortex and raphe reticular formation but not from red nuclei

To further investigate whether bPAC treatment leads to preservation or regeneration of the CST, we employed a retrograde tracing approach. This method overcomes a key limitation of anterograde labeling techniques, which typically capture only a small fraction of

CST fibers from the lumbar segments⁴⁰, while also enabling the examination of additional descending motor pathways beyond the corticospinal tract. Lumbar injections of rAAV2-Syn1-eGFP (14 days after injury) caudal to the injury site, label supraspinal projection neurons with spared axonal tracts across the injury (Fig. 4A).

We analyzed the number of retrogradely-labeled neurons in the primary motor cortex (bregma from +2 to -3; Fig. 4B). We observed a

Fig. 2 | Passive and firing properties of layer 5 pyramidal neurons from motor cortex of uninjured, Control (injured) and bPAC (injured) rats. **A** Representative examples at resting membrane potential in basal conditions. **B–E** passive electrophysiological membrane properties. **B** Resting membrane potential (Vm) of Layer V neurons at basal conditions. **C** Membrane capacitance (Cm) of neurons and **(D)** their membrane resistance (Rm). **E** Membrane time constant. **F** Representative examples trace of neurons in response to the protocol shown on the right, no hyperpolarizing sag is observed in response to 500 ms, -100 pA and illustrating the firing rate differences. **G** Representative example traces of the firing threshold and firing rate (top) in response to 19 depolarizing pulses protocol, 10 pA increments, 700 ms duration (bottom). The threshold current at rheobase for each group is represented at the bottom accordingly and the AP delay is marked up with a double arrowhead line for each group on top of the AP firing. **H** Quantification of the firing

rate in response to 500 ms, 250 pA depolarizing current step, applied in **(F)**. **I** Quantification of the AP firing threshold. **(J)** lower intensity of the threshold current needed for eliciting one first AP firing (at rheobase) in the bPAC-treated group. **K** Quantification of the AP delay. **L** and **M** Input-output curves (e.g., see at 20 and 50 pA in **L**). Statistics performed in **(B–D** and **H–L)** Ordinary one-way ANOVA followed by Holm-Sidak multiple comparisons post hoc test. Statistics performed in **(E** and **M)** Kruskal-Wallis test followed by Dunn's multiple comparisons post hoc test. Data is presented as a mean \pm SEM with statistical significance set as * $p < 0.05$, ** $p < 0.01$, *** $p < 0.001$ and **** $p < 0.0001$, n.s.: not significant. Sample size corresponds to individual neurons recorded across three biological replicates per group. Source data and exact P values for each comparison are provided as a Source Data file and Supplementary table 1.

substantial number of labeled corticospinal neurons in Layer V of the motor cortex of uninjured rats (91.6 ± 2 neurons/brain slice; Fig. 4B, right panel). The thoracic dorsal hemisection dramatically reduced the number of eGFP corticospinal retrogradely labeled neurons ($p \leq 0.0001$, for uninjured Control vs. bPAC and uninjured control vs Injured Control, Tukey's test). Strikingly, while we found sparse eGFP cells in injured Control animals (0.4 ± 0.4 neurons/brain slice, $n = 6$ rats), bPAC rats showed significantly higher numbers of labeled neurons (8.8 ± 7.4 neurons/brain slice, $n = 6$ rats) in the primary motor cortex ($p = 0.03$ for injured Control vs. bPAC, Tukey's test; Fig. 4B).

Unexpectedly, while almost 100% of retrogradely-labeled corticospinal neurons in uninjured Control rats located in Layer V, injured Control and bPAC rats possessed eGFP neurons in additional layers: 47% in Layer V, 37% in Layer II-III, 7.7% in Layer IV, 4.7% in Layer VI, and 2.4% in Layer I, effect that was also reported by Zhigang He et al.⁴¹. However, layer distribution analysis revealed no significant difference between bPAC and injured Control, indicating the injury dependence and bPAC-independence of this effect (Supplementary Fig. 4).

This result evidences a greater presence of CST axons reaching spinal segments caudal to the injury site in bPAC-stimulated animals compared to Controls, due to either enhanced regeneration of the damaged tracts or improved preservation of the non-transected ventral CST.

Next, we also explored the number of retrograde-labeled neurons in additional supraspinal nuclei with a known relevance in locomotor recovery^{42,43}—such as the red nuclei, caudal raphe nuclei, and the reticular formation.

The red nuclei, located in the midbrain, is the niche for rubrospinal neurons that project as the rubrospinal tract (RST) into the dorsolateral funiculus of the spinal cord⁴⁴. Injured rats displayed very few retrogradely-traced neurons compared to uninjured Control rats (Fig. 4C). Numbers of eGFP-labeled neurons in the red nuclei showed no significant differences between bPAC and Control rats (Fig. 4C), suggesting that the RST does not actively participate in bPAC-mediated functional recovery.

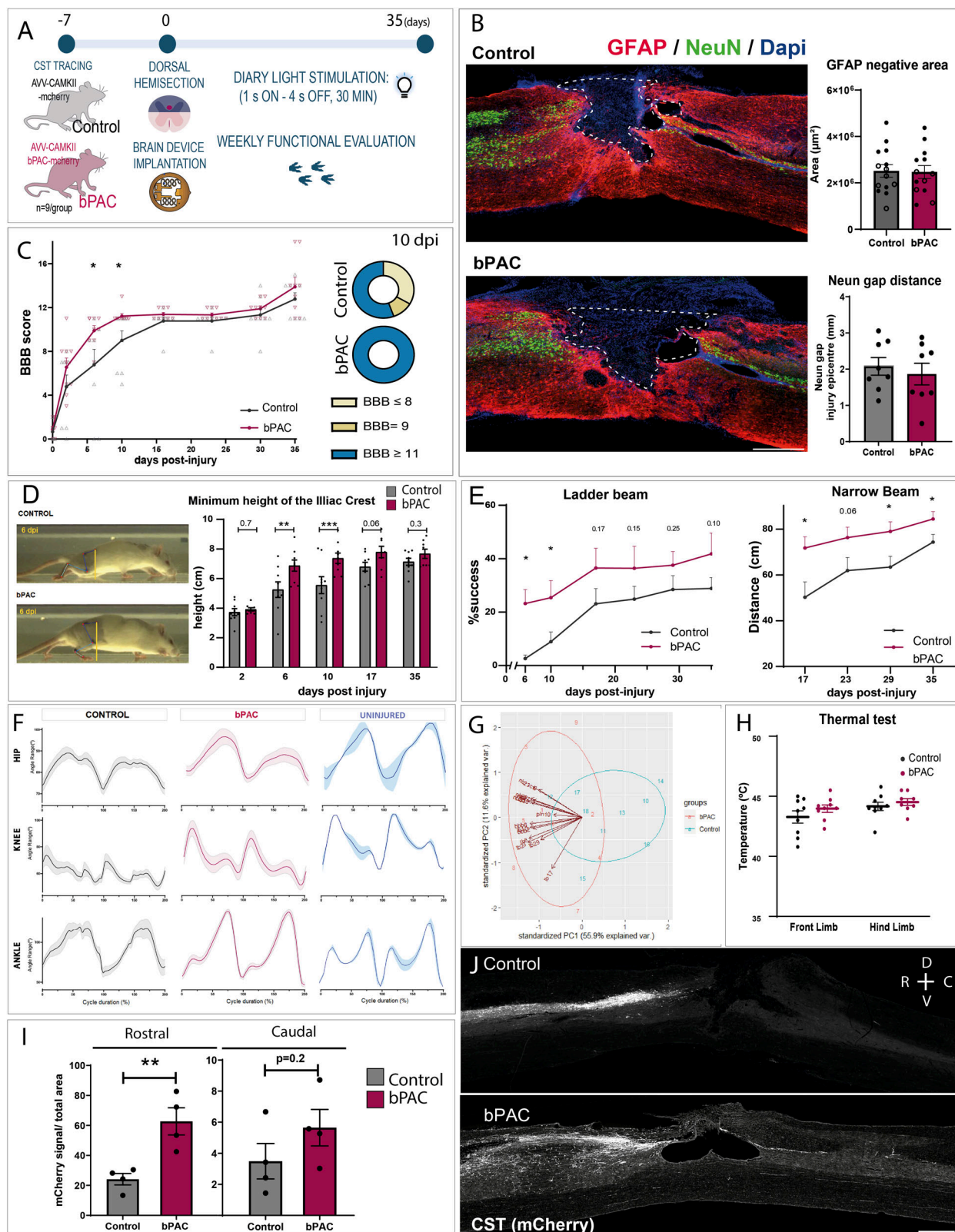
Caudal to the red nucleus, additional motor centers reside within the brainstem. The medullary reticular formation represents a complex network of motor nuclei, including the gigantocellular reticular nuclei and the caudal raphe nuclei, which project caudally to the ventrolateral funiculus of the spinal cord as the reticulospinal and raphespinal tracts, respectively¹⁰. Diffuse boundaries between these regions make their separate analysis challenging^{9,43,45}; therefore, we have characterized them together as “raphe-reticular” formation. Dorsal hemisection partially transects the medullary RtST and RpST, leaving some undamaged tracts; in agreement, eGFP-labeling was detected in the raphe reticular formation even in injured rats (6.9 ± 4.6 neurons/brain slice, Fig. 4D). Interestingly, bPAC rats displayed higher numbers of eGFP-labeled neurons in the raphe-reticular formation than Control rats (21.3 ± 11.9 neurons/brain slice, p value = 0.06 for bPAC vs Control, Tukey's test, Fig. 4D).

To explore the functional relevance of each supraspinal motor center in the recovery of locomotion, we correlated the number of retrogradely-labeled neurons in each brain region to BBB scores. eGFP cell counts in the motor cortex or red nuclei did not significantly correlate with BBB scores (Fig. 4E, upper and middle panels respectively). Remarkably, the number of retrogradely-labeled neurons within the raphe-reticular region did significantly correlate with BBB scores at 7- and 10-days post-injury (timepoints with the most significant functional difference between bPAC and Control) (Fig. 4E, lower panel, dark blue). This result unveiled the functional relevance of the brainstem descending pathways in bPAC-mediated functional recovery from SCI.

bPAC stimulation mediates serotonergic tract regeneration which directly correlates with functional recovery after SCI

Serotonergic neurons are the major cellular component of the raphe nuclei, projecting 5-hydroxytryptamine (5-HT) axons to the spinal cord. Serotonergic innervation caudal to the injury site has proven to be crucial for motor recovery⁴⁶. Thus, we further explored the serotonergic tract state in the spinal cord by direct serotonin 5-HT immunohistochemistry. 5-HT immunostaining allowed the visualization of serotonergic tracts mainly innervating ventral horn neurons of the spinal cord (Fig. 5A). bPAC rats showed a significantly increased level of caudal 5-HT positive signal compared to injured Control animals (Fig. 5A and B) (p value = 0.029, unpaired t-test), confirming the significantly enhanced regeneration of the serotonergic tracts. Importantly, the amount of caudal 5-HT staining significantly positively correlated with better performance in several locomotor tests (BBB scores: $p \leq 0.001$, Narrow beam: $p \leq 0.05$, Ladder beam: $p \leq 0.05$ and inclined plane: $p \leq 0.0001$), while it did not correlate with thermal test measurements or the injury size measured as the GFAP negative area (Fig. 5C). 5-HT terminals innervate and establish synaptic contacts with choline acetyltransferase (ChAT) positive motor neurons of the ventral horn, which may account for the implication of the serotonergic tract in motor recovery after SCI (Fig. 5D)^{47–50}. Moreover, immunostaining for the serotonin transporter (SERT), an additional marker of serotonergic innervation, further confirmed a significantly higher caudal-to-rostral SERT ratio in bPAC-treated rats compared to controls (Fig. 5E and F), supporting enhanced serotonergic fiber presence caudal to the injury with serotonin uptake capability. Consistently, HPLC determination of 5-HT levels in spinal cord extracts showed a trend toward higher caudal-to-rostral 5-HT concentrations in bPAC animals compared to control (0.51 ± 0.27 vs. 0.14 ± 0.11 μ M/mg protein, respectively; $p = 0.08$, Mann–Whitney test, Fig. 5G).

Altogether, this data suggests active participation of serotonergic tracts in motor recovery through direct motor neuron interaction and highlights the functional importance of bPAC-mediated serotonergic tract modulation.



bPAC stimulation can mediate trans-neuronal activation of brainstem neurons

We next aimed to investigate how bPAC stimulation and cAMP induction in the motor cortex might influence serotonergic neurons. Given that the pyramidal tracts (py) innervate raphe and reticular areas through the corticobulbar pathway, we hypothesized that bPAC stimulation could serve as a pushing input to activate the spinal-

projecting neurons at the brainstem level. Numerous corticobulbar projections arise from the pyramidal tracts by as detected by anterograde tracing from the motor cortex (Fig. 6A, left, red) in both, Control and bPAC groups. By analyzing the py innervation in density heatmaps computed from immunostaining images we found higher innervation in the raphe (RMg, RPa) and gigantocellular nuclei (GiA, LPGi), while other areas such as the medial laminsc (ml) remained

Fig. 3 | bPAC stimulation promotes early and sustained locomotor recovery after SCI. **A** Experimental design for functional evaluation in bPAC and Control SCI rats for 35-day after dorsal hemisection ($n = 9$ rats/group). **B** Immunostaining images for GFAP (red) and NeuN (green) and the quantification of both GFAP negative area and NeuN gap distances as indicators of injury extension. **C** Pie-charts of the percentage of Control and bPAC rats with or without weight support and plantar stepping capacity at ten days post-injury. **D** Measurement of iliac crest height as an indicator of weight-bearing capacity ($p = 0.002$ at 6dpi and 0.0007 at 10 dpi). **E** Performance of bPAC and Control rats in ladder (left) and narrow (right) beam tests ($p = 0.02, 0.06, 0.02$ and 0.045 at 17, 23, 29 and 35 dpi respectively). **F** Hind-limb kinematics at the endpoint of the experiment (35 days) in Control and bPAC rats compared to uninjured Control rats as shown by the hip (top), knee

(middle), and ankle (bottom) angle range. **G** Principal component analysis of combined locomotor parameters in Control and bPAC rats; bbb: Basso, Beattie, Bresnahan test; pln: inclined plane test; nb: narrow beam test; lb: ladder beam test; ci: crest iliac height. Numbers indicate the days post injury; **H**) Thermal test of the front paws (as an internal control) and hind paws in Control and bPAC rats. **I** Quantification of CST state rostral and caudal to the injury as given by the area positive for the anterograde tracer (mCherry) ($p = 0.0077$). **J** Sagittal images of the CST state in control and bPAC rats (Scale bar:1000 μm). Data is presented as a mean \pm SEM with statistical significance set as $*p < 0.05$, $**p < 0.01$, and $***p < 0.001$ for comparisons two-tailed Fisher's LSD (C-E and H) or two-tailed unpaired t-test (I). Scale bars=1000 mm. Source data are provided as a Source Data file.

poorly innervated (Fig. 6A, right). Compared to Control rats, bPAC treated animals have higher density of corticobulbar projections in the raphe-reticular region, especially in the medial zone (Fig. 6A, right). Interestingly, bPAC rats displayed discrete but significant P-CREB induction in the raphe magnus nuclei compared to injured Control; which was also observed at the LPGi and GiA without reaching statistical significance (Fig. 6B, C). Higher levels of P-CREB in the brainstem correlated positively with higher levels of P-CREB in the motor cortex (Fig. 6D). Additionally, HPLC analysis of brainstem extracts revealed a trend toward elevated cAMP levels in bPAC-treated animals compared to controls (7.14 ± 0.78 vs. 3.78 ± 1.48 $\mu\text{M}/\text{mg}$ protein, respectively; $p = 0.06$, one-tailed t-test; Fig. 6E). Notably, the glutamate/GABA-aminobutyric acid (GABA) ratio, reflecting the balance between excitatory and inhibitory neurotransmission, was significantly increased in the brainstem extracts of bPAC animals (2.5 ± 0.2 in bPAC vs. 1.6 ± 0.1 $\mu\text{M}/\text{mg}$ protein in controls; $p = 0.029$, Man-Whitney test, Fig. 6F), indicating a pronounced shift toward excitation.

These results strongly suggest that local cortical bPAC stimulation in corticospinal neurons may also influence distal brain regions, particularly the brainstem, resulting in increased cAMP-dependent signaling (P-CREB activation) as well as increased excitatory/inhibitory (E/I) balance. Such neuromodulatory changes may support functional and structural remodeling of descending brainstem pathways, potentially leading to significant motor recovery following injury.

Motor cortex neurons synaptically contact with brainstem spinal-projecting neurons

To explore the potential cortico-brainstem synaptic interactions we use wheat germ agglutinin (WGA) as a transsynaptic neuronal tracer⁵¹ in the motor cortex of bPAC or Control rats following the design described in Fig. 6G. Pyramidal neurons effectively captured WGA in the injection zone (Fig. 6H), and WGA dotted-like staining was detected in cells of the raphe-reticular formation in both groups, demonstrating that the brainstem is synaptically integrated with the motor cortex (Fig. 6I). However, no significant differences were found for counts of all WGA-positive neurons in bPAC or Controls (Fig. 6J and Supplementary Fig. 5).

To unveil whether spinal-projecting neurons of the brainstem receive synaptic contacts from the motor cortex, we designed a double-tracing experiment that combined cortical WGA injections with lumbar injections of the retrograde tracer rAAV2-Syn1-eGFP in SCI rats (Fig. 6K). While some brainstem neurons displayed only single labeling with either WGA (Fig. 6L) or GFP (Fig. 6N), interestingly, 40.5 ± 10.0 % of the neurons retrogradely labeled from the lumbar spinal cord were also positive for WGA-dotted staining (Fig. 6M, O). No significant differences of double-positive cells at the brainstem were observed among groups.

This result demarks that a substantial proportion of the lumbar-projecting neurons of the brainstem are putative to receive synaptic inputs for the motor cortex following SCI. Thus, cortical inputs could be rerouted through this pathway to caudal segments of the spinal cord after CST injury. Thus, bPAC-mediated cAMP elevations in

corticospinal neurons may mediate the synaptic modulation of spinal-projecting population of neurons residing in the brainstem.

Serotonergic depletion by DHT treatment abrogates bPAC-induced functional recovery

To definitively investigate the relevance of serotonergic descending tracts for the observed functional recovery in bPAC rats we selectively deplete the serotonergic system by administration of 5,7-dihydroxytryptamine (DHT) via intraventricular injection, at the steady state in the functional recovery (22 days after SCI) (Fig. 7A). Ablation of serotonergic innervation using DHT is a well-established method, shown to be effective and specific, with no secondary effects in noradrenergic system when animals are pre-medicated with desipramine^{52–54}. Post-mortem analysis revealed that DHT efficiently depleted serotonergic inputs in the spinal cord, as shown by reduced 5-HT staining in lumbar (Fig. 7B) and sagittal (Supplementary Fig. 6) spinal cord slices of DHT-treated animals (referred as DHT +) compared to non-DHT-treated controls (DHT-). DHT treatment, did not affect other general markers of spinal cord tracts, such as phosphorylated neurofilament (P-NF), (Supplementary Fig. 6).

We assessed motor function by ladder beam test prior and six days after DHT administration. Of note, while bPAC rats demonstrated significantly higher scores than injured Control rats pre-DHT administration, after DHT treatment bPAC scores decline but Controls continued improving, dampening the initial differences (Fig. 7C, left graph). When expressed in terms of score increments (as the difference in the score pre- and post-DHT treatment for each animal) all bPAC rats yielded negative values (indicative of functional worsening) while injured Control rats rendered positive values (indicative of functional improvements) (Fig. 7C, right graph).

Overall, these results strongly suggest that the locomotor improvements induced by bPAC are, at least in part, mediated through the serotonergic descending pathway. Furthermore, the functional improvements observed in Control rats between 22–28 dpi, even after serotonergic depletion, may imply that other forms of neuroplastic reorganization—beyond the serotonergic tracts—are occurring at this stage.

Discussion

SCI occurs in an instant, dramatically disrupting brain-to-muscle neuronal circuits that, in humans, will not recover in a lifetime. Despite this, most cases exhibit a significant portion of uninjured remaining tracts, leaving the door open for a certain extent of spontaneous functional recovery occurring during the first weeks-months after the trauma⁵⁵. Locomotor improvement is possible due to either structural or functional injury-induced neuronal plasticity that may occur at different CNS levels, including the cortex, the brainstem and the spinal cord⁵⁶. Deciphering how neuronal circuitry at all these levels reorganize to take over damaged pathways' functions remains a daunting yet essential challenge for developing new neuromodulatory therapies that could better direct the reorganization process. Recently, efforts have mainly focused on understanding the plastic reorganization of CST at the spinal level^{14,57}, leaving the mechanisms

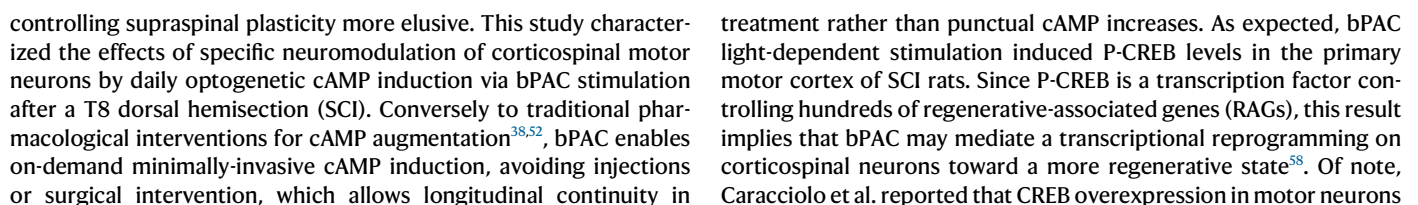


Fig. 4 | bPAC stimulation increases retrogradely-labeled neurons in the motor cortex and raphe-reticular formation, but not in the red nucleus. The counts of retrogradely-labeled neurons in the raphe-reticular formation directly correlated to improved locomotion. **A** Experimental design for analyzing the supraspinal descending tracts by retrograde tracing using AVV2-Syp-eGFP injections in the lumbar spinal cords in uninjured Control, injured Control, and bPAC rats. **B–D** Representative images (left) of retrogradely-labeled neurons (eGFP) observed in the **B**) motor cortex ($p < 0.0001$, for uninjured vs control and bPAC and 0.0366 for bPAC vs control), **C** red nuclei ($p < 0.0001$, for uninjured vs control and bPAC and 0.6 for bPAC vs control), and **D**) raphe-reticular formation ($p < 0.0001$, for uninjured vs control and bPAC and 0.06 for bPAC vs control) and their

respective quantification. Each data point represents a biological replicate.

E Pearson correlations between the counts of retrogradely-labeled neurons in the motor cortex (top), red nuclei (middle), and raphe reticular formation (bottom) and the BBB scores at 1-, 2-, 3-, 4-, 7- and 10-days post-injury. The graph shows P values for each comparison (one-tailed Pearson test); Color intensity indicates statistical significance as described in the legend. Scale bars= 1000 μm (for low magnification images) and 500 μm (for high magnification images). Data is presented as a mean \pm SEM for one-way ANOVA comparisons and Tukey's post-test with statistical significance set as * $p < 0.05$, *** $p < 0.001$, and **** $p < 0.0001$. Source data are provided as a Source Data file.

promoted motor recovery after stroke by inducing cortical re-mapping, while CREB inactivation turned off the functional recovery⁵⁹, providing evidence that CREB phosphorylation in the motor cortex suffices to drive motor recovery. We also demonstrated that cAMP induction by bPAC stimulation led to increased c-Fos immunostaining in Layers IV and V of the motor cortex, possibly by generating calcium waves through cAMP-gated calcium channel³¹, indicating that bPAC maintained neuronal activity of corticospinal neurons after SCI.

Ex vivo patch-clamp experiments have shown that corticospinal neurons from injured Control rats exhibited increased membrane capacitance and decreased membrane resistance along with reduced excitability (lower firing rate and increased AP delay) compared to the uninjured group, indicating impaired neuronal function. Strikingly, bPAC treatment effectively counteracted these injury-induced changes, restoring both the passive membrane properties and excitability parameters of pyramidal neurons to levels resembling those observed in the uninjured condition.

In agreement, the evaluation of the locomotor outcomes of SCI rats revealed that bPAC stimulation improved functional recovery after injury. Specifically, we described that the greatest differences in BBB scores between bPAC and injured Control animals occurred early compared to the timing of other SCI therapies⁶⁰, supporting the importance of early interventions for a better clinical prognosis. At 6- and 10-days post-injury, bPAC stimulation increased the weight-bearing ability of the rats, thus leading to significant differences in BBB scores and height of the iliac crest. Both observations indicate the involvement of the serotonergic tract, as 5-HT tracts have shown to be crucial for hindlimb weight support after spinal cord injury^{11,61,62} and therapies targeting raphespinal tract regeneration have reported very early functional recovery⁶¹. Despite the earliness of the bPAC-mediated functional recovery, the locomotor differences between bPAC and injured Control animals are sustained through the experiment, as shown by more challenging tests (ladder, narrow), which require more advanced postural control, front-limb hind-limb coordination and muscular tone³⁷, reinforcing the relevance of early regenerative intervention for improvements on skilled motor tasks.

Alongside the functional benefits of bPAC stimulation, we observe a deleterious effect derived from long-term bPAC stimulation –42% (11/26) of bPAC rats included in this study developed seizure episodes during stimulation. In long-term experiments, 3 out of 9 rats developed seizure episodes several minutes after the beginning of the stimulation routine by day 30 of daily stimulation. By day 35 of the experiment, 9 out of 9 animals developed seizures during the first 5 min of stimulation. In contrast, in short-term experiments of this study, only 8% (2/26 rats) developed seizures at early time points, 7 days of stimulation. Supplementary Table 2 contains a detailed report of seizure apparition. Seizures stopped shortly after removing animals from the stimulation cage, and we detected no spontaneous seizures in the elapsed time between stimulations nor Control rats, indicating that seizures depended on bPAC hyperexcitability. Similarly, deletion of the *PTEN* (phosphatase and tensin homolog) gene – which has been considered for years the most efficient means to induce CST regeneration and motor improvement after SCI^{63,64} – also

led to spontaneous epileptic seizures in 82% of animals⁶⁰. Further refinement of the temporal windows of bPAC stimulation may prevent the development of seizures while retaining the functional benefits, casting some optimism for this therapy.

To investigate the mechanisms underlying functional recovery in bPAC-stimulated rats, we examined the state of the CST following injury using both anterograde and retrograde tracing techniques. bPAC treatment resulted in an increased CST anterogradely labeled axonal area rostral to the lesion, which may reflect enhanced sprouting, reinnervating spinal interneurons within the gray matter. Additionally, bPAC stimulation led to a higher number of retrogradely labeled neurons from the lumbar spinal cord in the motor cortex, suggesting that a subset of cortical projections still reach sublesional regions of the spinal cord post-injury. This preservation or regeneration of descending inputs raises the possibility that bPAC activation could influence lumbar spinal circuits, including the central pattern generator (CPG), potentially contributing to locomotor recovery⁶⁵. However, this interpretation remains inconclusive, with the limitation of the anterograde sensibility detection and by the lack of significant correlation between the number of retrogradely labeled cortical neurons and functional outcomes measured by BBB scores.

Retrograde tracing studies also allowed the study of other descending tracts with supraspinal origins. bPAC stimulation increased the number of retrogradely-labeled neurons in the raphe-reticular formation, which positively correlated with BBB scores at days 7 and 10, remarking its locomotor implication. This finding suggests that bPAC promotes the regeneration of transected or the preservation of non-transected RpST and RtST, since increased sprouting would not explain the difference in number of retrogradely-labeled neurons (although sprouting is not excluded). Accordingly, the serotonergic tract, descending from serotonergic neurons of the raphe-reticular formation, displayed increased caudal/rostral ratio in 5-HT or SERT immunostaining in bPAC-stimulated animals compared to injured control rats.

The effects of bPAC stimulation on serotonergic tracts raised an open question: how does primary bPAC stimulation in corticospinal neurons trigger functional effects mediated by a secondary non-originally-targeted tract? In this regard, Leibinger et al. reported the transneuronal delivery of Hyper Interleukin 6 (hIL6) and JAK/STAT activation of raphespinal neurons after the adenoviral delivery of hIL6 overexpression into the motor cortex, resulting in raphespinal regeneration and functional recovery⁵⁴. Similarly, we observed a moderate induction of P-CREB in the raphe magnus nuclei of bPAC-treated rats, which correlated with P-CREB activation in the primary motor cortex. In addition, we described a trend toward elevated cAMP concentrations along with a significantly increased glutamate/GABA ratio in the brainstem, indicating a shift in the excitatory/inhibitory (E/I) balance. Together, these findings support the idea that cortical stimulation can remotely modulate subcortical motor centers such as the raphe nuclei, potentially contributing to functional reorganization and recovery after SCI.

In agreement to that, we reported copious cortical projections arising from the pyramidal tract and innervating the raphe-reticular formation. bPAC stimulation slightly altered the distribution of

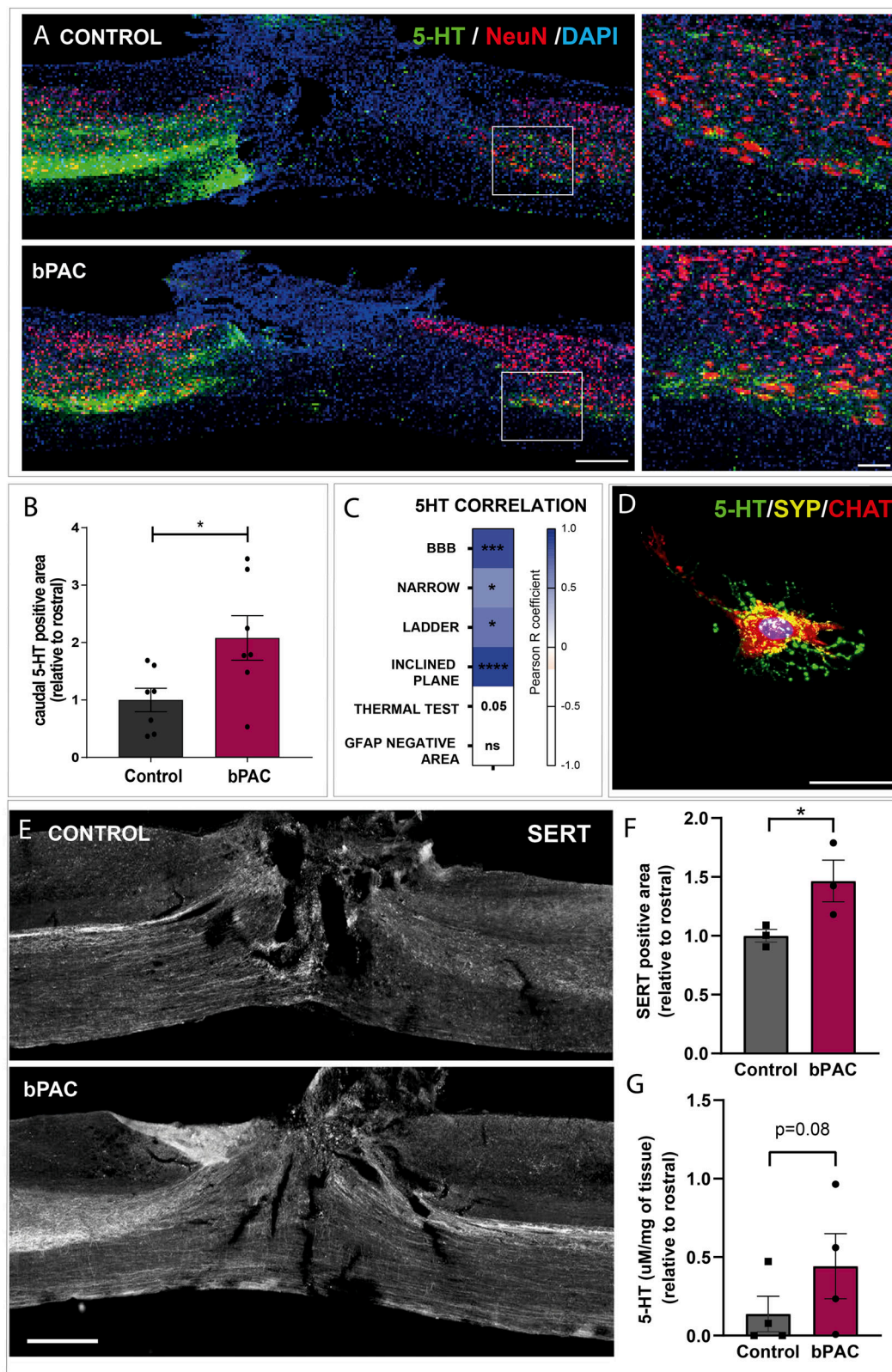
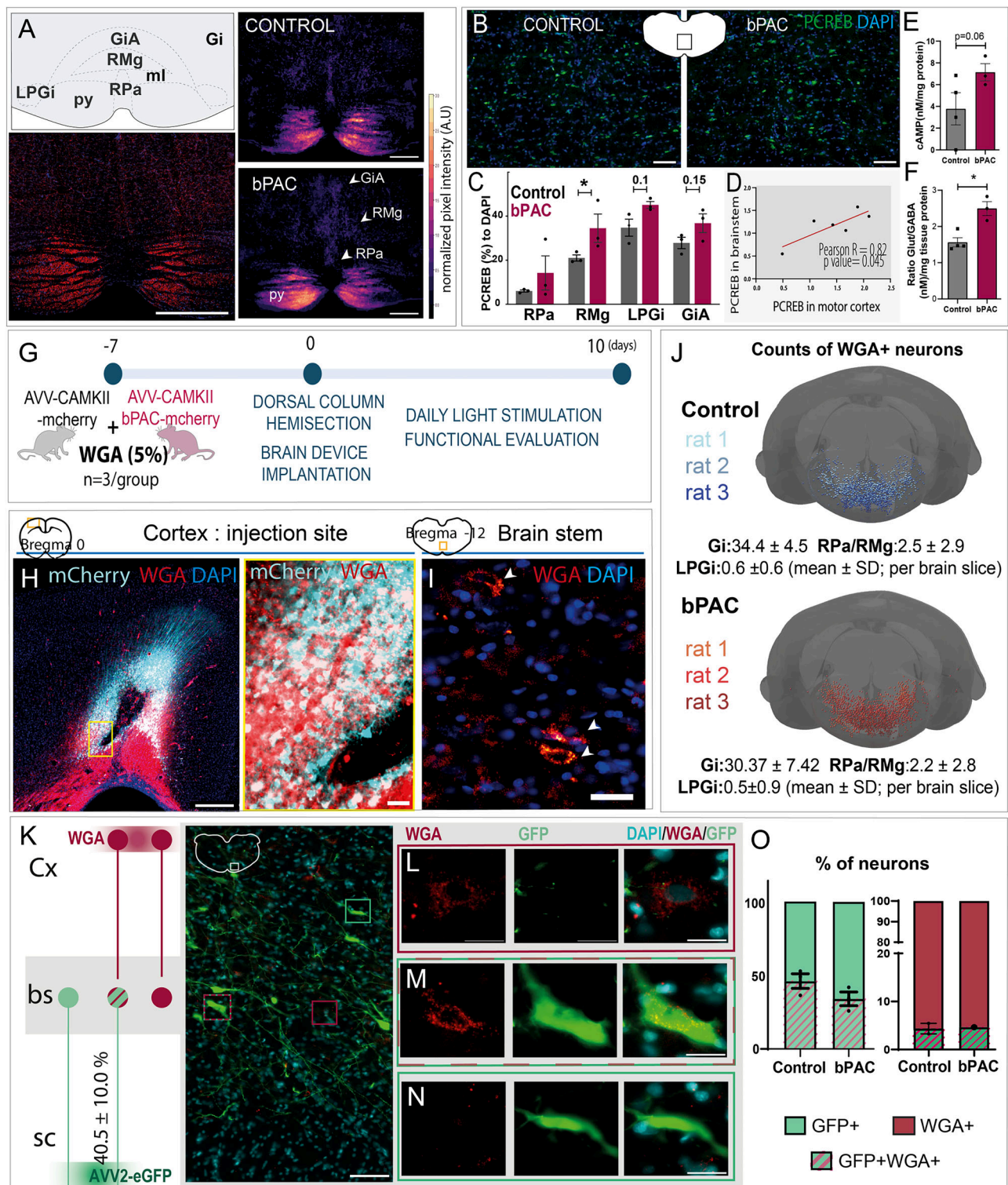


Fig. 5 | bPAC stimulation induces serotonergic tract regeneration/preservation across the injury correlating with improved functional recovery.

A Representative images of 5-HT immunostaining (green) in sagittal sections of the spinal cords in Control and bPAC rats 35 days post-injury at low and high magnifications (Scale bars = 1000 and 200 μm , respectively) and **(B)** its quantification, $n = 7$ rats/group, $p = 0.029$. **C** Pearson correlations between several locomotor tests and the amount of caudal 5-HT staining. Color code indicates the Pearson R coefficient, as shown in the legend; P values for each correlation are indicated inside each cell. **D** Representative image showing a ChAT+ motor neuron (red) innervated

by serotonergic axons (green) and synaptic contacts (yellow) between them. Scale bar = 50 μm . This observation was consistent across all biological replicates.

E Representative images of serotonin transporter (SERT) immunostaining in sagittal sections (Scale bars=1000 μm) and **(F)** its quantification, $n = 3$ animals/group, $p = 0.03$. **G** Quantification of 5-HT levels ($\mu\text{M}/\text{mg}$ of in spinal cord tissue, ratio caudal/rostral) by HPLC, $n = 4$ animals/group, $p = 0.08$. Data is presented as a mean \pm SEM for either two-tailed t-test **(B)**, two-tailed Pearson correlation **(C)**, one-tailed t-test **(F)** or one-tailed Man-Whitney test **(G)**, with statistical significance set as $*p < 0.05$. Source data are provided as a Source Data file.



corticobulbar projection, with higher densities observed at the raphe magnus and GiA nucleus. We found that at least 40% of the brainstem neurons that maintain axonal projections to the lumbar segment of the spinal cord following a thoracic dorsal hemisection are synaptically connected with neurons in the motor cortex. Together, these results strongly suggest the brainstem as an important transshipment station for rerouting cortical inputs into intact descending RpaST/ReST after an injury affecting the CST.

Cortico-brainstem or corticobulbar projections represent an ancient evolutionary pathway present in multiple species, including

rodents¹¹, cats⁶⁶, pigs⁶⁷, and primates⁶⁸. Del Cerro et al. demonstrated that the porcine CST only reached the T6 spinal cord level and relied on cortico-brainstem interaction to drive inputs to the lumbar segment even in naïve conditions⁶⁷. Additionally, Courtine et al. reported that silencing of reticulospinal neurons of the vGi during channelrhodopsin 2 cortical stimulation abolished evoked leg muscle potentials in contusion rodent models, indicating that these neurons relayed the cortical command to hind-limb motor neurons after SCI¹¹. These two studies highlight the relevance of cortico-brainstem interaction in both injured or uninjured scenarios.

Fig. 6 | bPAC stimulation may be transduced from the motor cortex to brainstem neurons. **A** Representative example of an original (lower left) image and computed heat maps showing the density of corticobulbar projections into the brainstem for injured Control (right, upper) and bPAC rats (right, lower). Heat maps integrate data from 4 bPAC and 5 control biological replicates. Scale bar = 200 μ m. **B** Representative images of P-CREB staining in brainstem slices at higher (left upper and lower) and lower (right upper and lower) magnifications in injured Control and bPAC rats. Scale bars = 500 (left) and 100 (right) μ m. **C** Quantification of the proportion of P-CREB relative to DAPI in each region in injured Control and bPAC rats, $n = 3$ animals/group, $p = 0.04$ for RMg. **D** Correlation between P-CREB in the motor cortex and brainstem. **E** Quantification of cAMP levels, $n = 4$ rats/group, $p = 0.06$ and **F** Glutamate/GABA concentrations in brainstem (μ M/mg of tissue) by HPLC, $n = 4$ rats/group, $p = 0.02$. **G** Experimental design for studying synaptic connections between motor cortex and brainstem in injured Control and bPAC rats. **H** Representative images of the WGA and AVV injection sites at low (left) and

high (right) magnifications. Scale bars = 500 (left) and 50 (right) μ m.

I Representative images of brainstem region displaying WGA-positive cells. Scale bar = 50 μ m, $n = 3$ rats/group. **J** 3D reconstruction of WGA-positive cell counts and distribution in the brainstem region in injured Control and bPAC rats. Each brain representation includes data from three animals. Counts of WGA-positive neurons are expressed as mean \pm SD. **K** Experimental schema for the double-tracing experiment and representative images showing different labeled populations within the brainstem, $n = 3$ rats/group, Scale bar = 200 μ m. **J–L** High-magnification images of **(L)** WGA + GFP, **(M)** WGA + GFP+ and **(N)** WGA-GFP+ neurons in the brainstem. Scale bar = 50 μ m. **O** Graphs showing the percentage of double-positive neurons from the GFP+ (left) and WGA + (right) populations, $n = 3$ rats/group. Data is presented as Mean \pm SEM for comparisons using two-tailed multiple t-test (**C**, **O**), two-tailed Pearson correlation (**D**), one-tailed t-test (**E**) or one-tailed Man-Whitney test (**F**), with statistical significance set as $*p < 0.05$. Source data are provided as a Source Data file.

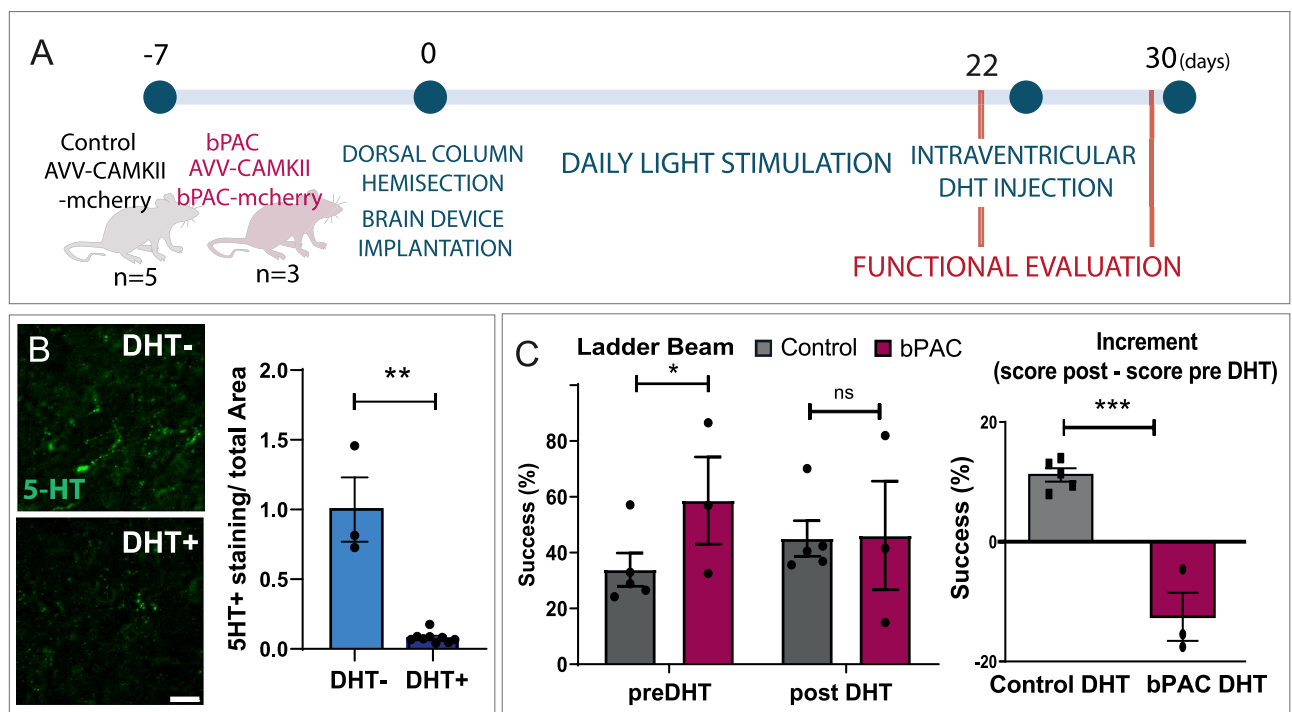


Fig. 7 | Serotonergic depletion by DHT treatment abrogates bPAC-induced functional recovery after SCI. **A** Experimental design to study serotonergic involvement in bPAC-mediated functional recovery. DHT treatment was applied to bPAC and Control rats 22 days after SCI, and their locomotor skills were evaluated before and 6 days after treatment. **B** 5-HT immunostaining in lumbar spinal cord slices of non-DHT-treated controls (denoted as DHT-) and DHT-treated rats (denoted as DHT+, both bPAC and Control rats) and its quantification. Scale bar =

50 μ m. Each data dot represents a biological replicate, $n = 0.009$. **C** Functional evaluation pre- and 6 days post-DHT injections expressed as the absolute achieved score in the ladder beam test (left, bPAC preDHT vs Control preDHT: $p = 0.02$ and bPAC postDHT vs control postDHT: $p = 0.55$) or the increment score post-to pre-DHT treatment (right, $p = 0.0004$). Data is presented as Mean \pm SEM, two-tailed Kolmogorov-Smirnov test (**B**), two-tailed t-test (**C**); $*p \leq 0.05$, $**p \leq 0.01$, $***p \leq 0.001$, ns=not significant. Source data are provided as a Source Data file.

Last, we evaluated serotonergic tract implication in bPAC-mediated functional recovery in loss-of-function experiments using DHT. This neurotoxin previously served to demonstrate a serotonergic role in therapy-mediated motor outputs^{53,54}. Interestingly, DHT administration worsened the performance of bPAC rats in the ladder beam test, rendering the scores to control injured rat levels. This finding strongly supports the involvement of serotonergic descending pathways in bPAC-induced locomotor recovery. However, it is important to note that serotonergic depletion at this stage of recovery (22 days post-injury) resulted in modest motor impairment, trackable in skilled motor tests, but no detectable motor deficits in open field walking. These observations suggest the implication of spontaneous plasticity of other tracts in the progressive recovery observed in bPAC and control injured rats.

Of note, our data does not exclude the participation of additional supraspinal or propriospinal pathways in a bPAC-mediated mechanism of action. Here, we reported certain insight into the effect of bPAC stimulation on the corticospinal and reticulospinal tract, which has not been thoroughly studied and deserves further exploration. The experiments presented here lay the groundwork for future optimization of bPAC-based therapies and further exploration of additional undescribed mechanisms.

To sum up, the cortico-serotonergic tract may provide a more regenerative descending pathway parallel to the more sophisticated but less regenerative corticospinal tract. Overall, this study highlights the relevance of cortico-brainstem plasticity for functional recovery after SCI. Importantly, RpST and RtST tracts are likely to remain partially intact in human SCI⁶⁹ due to their ventral anatomical location^{42,70}.

In the light of that premise, future therapies targeted to reroute cortical commands into spare brainstem descending circuits may possess more clinical relevance than those attempting to promote vague CST regeneration at the injury level.

Methods

Primary cortical neuron culture, cAMP determination, calcium dynamics

Cortical neurons were harvested from E14.5 fetal Sprague Dawley rats. Briefly, cortices were dissected from the brains and enzymatically dissociated using trypsin-EDTA (0.05%, 25300-054, Gibco). Neurons were then counted and seeded on poly-D-lysine pre-coated plates using a plating medium (containing DMEM High Glucose (SH30243.01, Cytiva), 10% fetal bovine serum, and 1x penicillin/and streptomycin (P/S)). After 2 h, the plating medium was changed to neuronal medium containing Neurobasal (21103-049, Gibco), B27 (17504-044, Gibco), 200 mM Glutamax (35050061, Gibco) and 1x P/S. To transduce neurons with our protein of interest, either AVV1-CAMKII-mCherry or AAV2/9-CAMKII-bPAC-mCherry were added to control or bPAC conditions at a multiplicity of infection (MOI) of 10^9 . Cells were incubated at 37°C at 5% CO₂ in dark conditions.

For cAMP determination, one week after the neurons were exposed to blue light (480 nm, 90 s of 20 mW/cm²) using an optogenetic stimulator for in-vitro experimentation (OSIVE)⁷¹ to induce bPAC activity. The stimulation parameters were selected to achieve a saturating effect of cAMP levels according to previous reports reporting that cAMP levels reached a plateau after bPAC exposure of 60 s of 6 mW/cm² blue light³⁰.

Immediately after stimulation, reactions were quenched by removing the culture medium and adding 0.4 M of perchloric acid (HClO₄). Next, cells were collected by scraping, homogenized by sonication, and centrifuged at 20,000 rpm at 4 °C for 10 min. Supernatants (containing cAMP extracts) were stored at -80 °C until used. Pellets (containing total protein contents) were resuspended in 1 M NaOH, and protein concentrations were measured using a BCA assay kit (23227, Pierce™ BCA Protein Assay Kit, Thermo Scientific). Based on previous reports, chromatographic parameters were optimized for an XBridge C18 2.1 × 75 2.5 mm (BEH Technology, Cat 186005626 Waters)⁷². The mobile phase composition was 0.1% formic acid in water and 100% acetonitrile. The conditions for the chromatographic run were: flow rate 0.4 ml/min, gradient: 0.5 min-100 %A; 1 min-10% A; 2.2 min-10% A, 2.3 min-100% A; 3.5 min-100 % A. The volume injected was 25 µl. Obtained cAMP concentrations were normalized to the total mg of protein in each experimental replicate. Three different experiments were performed (two replicates per experiment). Two outliers were identified by the ROUT method (Q = 1%). Group comparisons were made using the Welch t-test.

For calcium imaging, the cells were incubated with 3 µM Fluo-4 AM (Thermo Fisher) 30 min prior to the assay. Confocal Leica TSP-SP8 was used for time-lapse acquisition, equipped with resonant scanning mirrors to allow the adequate imaging speed required for real-time recordings of calcium⁷³ and maintaining adequate temperature and CO₂ levels for live imaging. The recording consisted in 1 image every 25 ms (40 frames/s) for 120 s. Two blue light stimulation (0.2 mW/cm², 470 nm) protocols were applied: stim 1 consisted in 500 ms pulses every 10 s and stim 2 consisted in 100 pulses of 90 ms on-10 ms off every 15 s, using the OSIVE Slim device⁷⁵. Calcium dynamics were measured as the increment of fluorescent given by Fluo-4AM defined as $F_x - F_0 / F_0$ (Fig. 1D) and the maximum fluorescence change defined as $(F_{max} - F_0) / F_0$ (Fig. 1D), quantified using LasX software.

Dorsal spinal cord hemisection and animal care

Young (2-4 months) Female Sprague Dawley rats were used in this study, given the ease of manual bladder drainage, which reduces the prevalence of urinary infections and supports a more stable body

weight after SCI than male rats⁷⁴. Animals were bred and housed with littermates under standard conditions with ad libitum access to food and water at the Animal Experimentation Unit of the Research Institute Príncipe Felipe (Valencia, Spain) in accordance with the guidelines of the European Communities Council Directive (86/609/ECC) and the Spanish Royal Decree 53/2013. Experimental procedures were approved by the Animal Care and Use Committee of the Research Institute Prince Felipe (2021/VSC/PEA/0032).

For surgical interventions, animals were subcutaneously treated with morphine (2.5 mg/kg) and anesthetized with 2% isoflurane.

A complete lesion model is highly disabling for the animal, and creates a significant barrier to regeneration, leaving no possibility for functional recovery. Moreover the majority of human SCI trauma results in incomplete injuries. For these reasons, most contemporary studies rely on partial injury models, which better mimic the clinical scenario. Dorsal hemisection, the most commonly used paradigm to study CST regeneration, generates a bilateral interruption of the descending motor pathways, including the dorsal aspect of the CST, the rubrospinal tract, and partially the raphespinal and reticulospinal tracts, while sparing the ventral CST. This sparing of ventral tracts allows for partial functional recovery, similarly to the contusion induced injuries, while reducing inconsistency and intra-animal variability inherent to the traumatic injury models.

For inducing SCI, a laminectomy was performed to expose the spinal cord at thoracic segment eight. Bilateral dorsal hemisection was performed by an incision of 1.1 mm in depth from the dorsal surface, leading to the total transection of the dorsal half of the spinal cord. After interventions, animals received post-surgical care consisting of subcutaneous injections of 5 mg/kg of Enrofloxacin (Baytril) for seven days, 0.1 mg/kg of buprenorphine twice a day for four days, and manual drainage of bladders twice a day until vesical reflex was recovered. Rat well-being was monitored, and endpoint criteria was applied if major signs of distress were observed.

Motor cortex injections

One week prior to SCI, excitatory corticospinal neurons were transduced to express bPAC by AAV9-CAMKII-bPAC-mCherry injections into Layer V of the motor cortex (coordinates from bregma: AP: 0, 2; ML: ±1.5; DV: -1.4, 6e12 VG/injection site). Control animals were injected with a bPAC-deficient vector (AVV1-CAMKII-mCherry, 114469, Addgene, Massachusetts, USA) or with the AVV9-CAMKII-bPAC L123R (AAV9-CAMKII-ΔbPAC), an inactive mutant construct, for anterograde tracing experiments. The CAMKII-bPAC L123R mutant construct was generated by point mutation mutagenesis following manufacturer instructions of QuickChange Lightning Site-directed Mutagenesis kit #210515-5, Agilent Technologies, using the primers Forward: CAGAGCCACCGGGTCCGGGAAAAGTACATG CCC and Reverse: GGGCATGTACTTTTCCCGCACCCGGTGGCTCTG) based on a previous report³⁹. Correct single point mutation was confirmed by Sanger sequencing. All vectors contained a red fluorescent reporter to allow the tracing of the descending corticospinal tracts. No significant differences in AVV1 and AVV9 serotype tropism have been previously reported when used in CAMKII construct in macaques, marmosets, and mice⁷⁵.

Light stimulation

On the same day of the injury, bilateral brain devices were implanted in all the rats to allow stimulation with blue light at 470 nm (NeuroLux; Northfield, USA). Devices were mounted sub-dermally on top of the animal's skull, and the µLEDs were placed beneath the skull and over each hemisphere of the motor cortex. The stimulation routine started one day after the SCI and was applied once a day until the end point consisting of 1 s on - 4 s off for 30 min at 8 W (procedure adapted from Chen et al.⁷⁶). During the stimulation, animals were placed in a cage connected to a power distribution control box

(Neurolux, Northfield, EE. UU) responsible for delivering wireless power to the implants.

Functional tests

To assess open-field locomotion, animals were recorded for 5 min once a week throughout the experiment while freely walking in an open space. Basso, Beattie, and Bresnahan (BBB) locomotor scale scores were analyzed by a blinded evaluator using the 21-point BBB locomotion scale⁷⁷.

Analysis of motor gait used the high-speed video system TSE MotoRater (TSE Systems, Bad Homburg, Germany), which records animal locomotion while crossing a transparent corridor simultaneously from three different perspectives (ventral, left, and right) in two different modalities: ladder skilled walking or overground walking. Animals were previously acclimatized to the setup prior to the test day. The ladder-walking animals were allowed to partially regain the ability to support their weight (for six days after injury) and then evaluated once a week throughout the experiment. Each animal's success rate was scored using the scale previously defined by Gerlinde et al.⁷⁸.

Animals with recovered trunk stability were evaluated for their ability to pass through an elevated narrow beam weekly from day seventeen post-injury until the end of the experiment. The narrow beam test measures the longer distance a rat can walk forward without making paw slips in at least three consecutive runs.

At the experimental endpoint, rats were passed through a transparent corridor (TSE MotoRater) to analyze finer motor kinematics. To track hind paw movement during locomotion, corporal landmarks of the hind-limb joints were marked on the shaved skin. SIMI Motion (SIMI Reality Motion Systems, Germany) software was used to acquire two-dimensional coordinates of each joint for each run. The step cycles for both paws in each run, defined as the transition between two ground contacts, were manually defined. Angle ranges for each joint were calculated and averaged across the two paws for two-step cycles.

Thermal test

Neuropathic pain is a usual side effect after CNS damage. A standard indicator of the presence of neuropathic pain in animal models of SCI is thermal hyperalgesia. Thermal test studies the animal behavior upon a thermal stimulus by observation of the hind paw withdrawal from a heat-radiant surface⁷⁹ (Ugo Basile Hot/Cold Plate, 35150). Thermal ramp starts at 25 °C and increases at a rate of 0.07 °C/s. Animals were instructed to maintain a quadrupedal position, being their behavior monitored throughout the test. The test concluded when the animals removed their paws from the plate as a reaction to the thermal stimulus, registering at that moment the temperature reached.

Retrograde tracing

Fourteen days after dorsal hemisection, animals were retrogradely traced from the lumbar spinal cord (L1). In brief, laminectomy was performed at the lumbar segments to expose the spinal cord. Four μ l at 1:2 dilution of pAAV-Syn1-eGFP; addgene#50465 were injected in eight different points (four points/hemisphere) at 1 mm of depth in the dorsoventral axis using the PV850 microinjector (World Precision Instruments, USA).

Sample processing and immunostaining

At the end of the experiment, the animals were overdosed with 100 mg/kg sodium pentobarbital and transcardially perfused with 4% paraformaldehyde (PFA) solution. Brains and spinal cords were carefully removed, fixed in 4% PFA, and stored in 0.1 M phosphate buffer (PB). Samples were cryopreserved in 30% sucrose in PB for at least seven days. Spinal segments of 1.8 cm in length (including the lesion epicenter) were cut into 35-micron thick slices in the sagittal plane using the Cryostat Microm HM550 (ThermoFisher, Germany). Brains were cut into 40-micron thick in the coronal plane.

Standard immunofluorescence staining was performed by incubation at 4 °C in the primary antibody solution in TBS + 5% donkey serum + 0.25% Triton for at least two nights and one night in the secondary antibody solution. mCherry/c-Fos/P-CREB/spinal 5-HT signals were amplified using the tyramide signal amplification (TSA) protocol⁸⁰. Primary antibodies used were anti-GFAP (α -Rb, 1:800, Z0334, DAKO, Denmark), anti-5-HT (α -Gt, 1:1000, AB_572262, Immunostar, Wisconsin, USA), anti-5-HT (α -Rb, 1:400, S5545, Merck Millipore, Massachusetts, USA), anti-SERT (α -Rb, 1:400, PC177L, Merck Millipore); anti NET (α -MS, 1:400, MA5-24647, Invitrogen), anti-c-Fos (α -Rb, 1:100, ab190289, Abcam, Cambridge, UK), anti-P-CREB (α -Rb, 1:100, 06-519, Merck Millipore, Massachusetts, USA) Anti-Choline Acetyltransferase, ChAT (α -Gt, 1:200, AB144P, Merck Millipore, Massachusetts, USA), anti-RFP/mCherry (α -Gp, 1:1000, 390 004 Synaptic systems, Göttingen, Germany). Secondary antibodies used for standard immunohistochemistry were Alexa Fluor-488, -555, or -647 conjugated antibodies (1:400, Invitrogen, Massachusetts, USA). Secondary antibodies used in TSA amplification immunohistochemistry were either Biotinylated Donkey anti-Rb or anti-Gp (706-065, Jackson ImmunoResearch, Cambridgeshire, UK) and either 555 (S21381, ThermoFisher, Massachusetts, USA) or 488 streptavidin (016-540-084 Jackson ImmunoResearch, Cambridgeshire, UK). Cell nuclei were counterstained with DAPI (1:1000, Sigma, Missouri, USA). Sections were mounted in Mowiol and imaged using an Aperio Versa scanner (Leica Biosystems, Germany). Images were visualized and analyzed with the Image Scope software or ImageJ software.

5-HT, mCherry for CST labeling and SERT quantification

For 5-HT and mCherry signal for CST labeling and immunohistochemical analysis in spinal cord the positive signal was quantified separately in the rostral and caudal regions of the injured spinal cords. To reduce the possible deviation of the cutting angle, 5-HT absolute data was then normalized to the ChAT positive area (as the zones putative for having 5-HT innervation). Next, the ratios from caudal to rostral were calculated for each slice ($n = 1-3$ slices/animal, $n = 7$ animals/group). For mCherry signal derived from anterograde tracing of CST, a complete series (including 8 tissue slices/animal, $n = 4$ animals/group) were included. The correlation of 5-HT measurements with locomotor parameters was studied by calculating Pearson coefficients for each pair of variables.

For SERT immunohistochemical analysis, the positive signal in rostral and caudal regions was relativized to total area of analysis per slice and the caudal to rostral ratios were calculated for each slice ($n \sim 5$ slices/animal, $n = 3$ animals/group). Rout's test ($Q = 5\%$) was performed to detect outliers.

c-Fos and P-CREB quantification

To quantify the amount of c-Fos along the cortical layers, first regions within the primary motor cortex in brain slices approximately at bregma -1 were selected. For each animal (three animals/group), three to five independent hemispheres were analyzed. All images were thresholded using the same parameters, and the histogram of mean gray value along the layers was displayed using the plot profile plugin of ImageJ both for DAPI and c-Fos. Then, c-Fos histogram profiles were normalized to DAPI, and all the images for each animal averaged to a single profile. Finally, the mean gray value of c-Fos encountered in each layer was calculated (two-way ANOVA Fisher's test).

For P-CREB quantification in the motor cortex, regions comprising the primary motor cortex were selected as defined by Paxinos and Watson atlas in brain slices at bregma -1.5 and measured (three animals/group, two hemispheres/animal), which was then normalized to the total DAPI counts. To quantify CREB phosphorylation in the brain stem, brain slices at bregma -11.88 were immunostained and imaged. Several regions of the raphe nuclei and the reticular formation were manually defined (according to the Paxinos and Watson atlas), and the

number of P-CREB+ nuclei and DAPI were quantified for each region. The average of P-CREB+ relative to DAPI was calculated (three animals/group; two slices/animal).

Determination of cAMP and neurotransmitters by LC-MS from tissue samples

The tissue concentration of serotonin, norepinephrine, cAMP, glutamate and GABA was measured by liquid-chromatography-mass spectrometry (LC-MS) as in Wang et al.⁸¹. An EXION (Shimadzu) HPLC system coupled to a mass spectrometry detection system consisting of a QTRAP 4500 triple quadrupole (AB Sciex, Ontario, Canada) equipped with electrospray ionization (ESI) ion source and controlled by the Analyst software, version 1.6.3, was used. The sample preparation proceeded as follows: samples were homogenized in H₂O (LC-MS grade) with 0.1% formic acid with a Poltron. Protein was precipitated by adding 10 μ L of trifluoroacetic acid to 50 μ L of sample. 30 μ L of the supernatant was injected in the HPLC, $n = 4$ animals/group, each sample was normalized to the total protein.

A Luna Omega Polar C18 (OOD-4760-AN) 100 \times 2.1 mm 3 μ m (100 Å) column from Phenomenex, at 35 $^{\circ}$ C, was used. The mobile phase consists of a two-phase gradient: 0.1% formic acid in water (A) and 0.1% formic acid in acetonitrile (B), as follows: 5% B 0–0.5 min, 5–80% B 0.5–5.0 min, 80% B 5.0–6.0 min, 80–5% B 6.0–6.1 min, 5% B 6.1–8 min, with a flow rate of 0.4 ml/min. ESI (electrospray ionization) ion source in positive ionization mode was used with curtain gas 30, GS1 40 and GS2 50, 500 $^{\circ}$ C and 4500 V in multiple reaction monitoring (MRM) mode with the following conditions for each metabolite: 1) Serotonin (5-HT): 177.1 m/z > 160 transition, RT 1.7 EP 10 CE 12 DP 80 CXP 13; 2) Norepinephrine (NE): 170 m/z > 152, RT 0.6 EP 10 CE 12 DP 40 CXP 13; 3) Glutamate: 148 m/z > 84, RT 0.6, EP 10, CE 2.1 DP 130, CXP 9 and 4) GABA: 104 m/z > 87, RT 0.6, EP 10, CE 15, DP 46, CXP 4, [RT: retention time; EP: entrance potential; DP: declustering potential; CE: collision energy; CXP: collision exit potential]. A standard curve for each metabolite was processed as the samples to calculate metabolite concentration in samples which was then relativized to the mg of protein in the tissue extract.

For cAMP analysis 50 μ L of the same tissue sample in H₂O was precipitated with an equal volume of 0.8 M perchloric acid. After centrifugation for 15 minutes at 17,000 g and 4 $^{\circ}$ C, 25 μ L of the supernatant was injected in the HPLC. Method described in ref. 82 was used with some modifications. Chromatographic separation was carried out at room temperature using the Luna Omega Polar C18 (OOD-4760-AN) 100 \times 2.1 mm 3 μ m (100 Å) column from Phenomenex. Mobile phase A consisted of 0.1% formic acid in water and mobile phase B was 100% acetonitrile. The following gradient elution profile was applied at a flow rate of 0.4 mL/min: 0.00 min: 90% A, 0.50 min: 90% A, 1.00 min: 10% A, 2.20 min: 10% A, 2.30 min: 90% A, 3.50 min: 90% A. Eluates were detected with the QTRAP 4500 triple quadrupole mass spectrometer (AB Sciex, Ontario, Canada) in the positive electrospray ionization (ESI) mode by multiple reaction monitoring (MRM) in the following conditions: Curtain gas 20 psi, GS1 45 psi, GS2 60 psi, Ion spray voltage 5.500 V, T $^{\circ}$ 600 $^{\circ}$ C, EP 10, DP 91, CE 35, CXP 10. The 330.08 to 136.10 transition was used for quantification of cAMP. Standard solutions of cAMP were prepared in 0.4 M of perchloric acid.

Ex vivo electrophysiological recordings

Coronal brain slices containing the motor cortex from both hemispheres were obtained from three-to-five-month-old female rats ($n = 3$). In brief, rats were deeply anesthetized with isoflurane (2%), decapitated, and the brain was quickly removed and placed in an ice-cold artificial cerebrospinal fluid (ACSF) containing 126 mM NaCl, 3 mM KCl, 1.25 mM NaH₂PO₄, 2 mM MgSO₄, 2 mM CaCl₂, 26 mM NaHCO₃, and 10 mM glucose (pH 7.2, 300 mOsm/L). Coronal slices (250- μ m thick) were obtained with a vibratome Leica VT1000S and maintained oxygenated (95% O₂/5% CO₂) in ACSF for at least 1 h before

use at room temperature. Recordings were conducted at 32–34 $^{\circ}$ C, and the slices were continuously superfused with oxygenated ACSF during the experiments.

Pyramidal neurons were visually identified at layer V of the motor cortex by their characteristic morphology and their distinctive electrophysiological responses to different stimulation protocols^{35,36}. These protocols were also used for the identification of GABAergic interneurons^{83–85} that were discarded from the study. Identification protocols comprised a two-step protocol (–100 hyperpolarizing pA and 300 depolarizing pA) and depolarizing ramp current injection (500 pA). Whole-cell patch clamp recordings were obtained under visual guidance by IR-DIC microscopy (Axio Examiner, Zeiss; Germany). Patch electrodes were pulled from borosilicate glass tubes having a resistance of 5–8 M Ω when filled with 110 mM potassium gluconate, 40 mM HEPES, 4 mM NaCl, 4 mM ATP-Mg, and 0.3 mM GTP (pH 7.2–7.3, 290 mOsm/L). Recordings were low-pass filtered at 3 kHz and acquired at 10 kHz with a patch-clamp amplifier (Multiclamp 700B) using pCLAMP 10.4 software (Molecular Devices) and stored using Digidata 1550 A and pCLAMP 10.4 software (Molecular Devices)^{85–87}. Spontaneous excitatory postsynaptic currents (sEPSCs) were recorded in voltage clamp configuration at –70 mV holding.

Passive membrane properties including membrane capacitance (C_m), membrane resistance (R_m), and membrane time constant (τ), were acquired with the Clampex membrane test tool, and amplifier readings in voltage-clamp mode. Resting membrane potential (V_m) was directly measured in current-clamp mode immediately after getting the whole-cell configuration. For the firing properties, the firing threshold was measured with Clampfit at the potential where the cell fired the first action potential (AP). The threshold current was measured at rheobase (when the neuron fired the first action potential) and the firing rate was assessed in response to a 250-pA depolarizing pulse delivered via patch pipette during 500 ms. For neurons that were firing spontaneously at basal V_m, a hyperpolarizing current was applied via patch pipette until the cell stopped firing to accurately detect the real firing threshold.

Spontaneous EPSCs were detected offline using a custom-made template in Clampfit 10.4 software (Molecular Devices, CA, USA) including around 20 averaged representative events. EPSCs parameters (amplitude and frequency) were analyzed and presented using GraphPad Prism 9.0 (GraphPad Software, USA) from 60 s-long sEPSCs recording segments. Statistical analysis was performed using GraphPad Prism 9.0 following outliers' detection (ROUT method, 1%) and Shapiro-Wilk normality test. Ordinary one-way ANOVA followed by Holm-Sidak's multiple comparisons test was used for parametric distributed data and Kruskal-Wallis test followed by Dunn's multiple comparisons test was used for comparisons of non-parametric data. Results are reported as mean \pm SEM and significance levels were set as follows: * $p < 0.05$, ** $p < 0.01$, *** $p < 0.001$, **** $p < 0.0001$.

WGA tracing

Wheat germ agglutinin (WGA) is commonly used as a neuronal tracer, given its ability to travel both anterogradely or retrogradely and to jump transynaptically⁸⁸. Injecting WGA into Layer V of the motor cortex allows tracing the synaptic connectome of corticospinal neurons. For that, 5% WGA Alexa Fluor 647 conjugated (W32466, Thermo Fisher, Massachusetts, USA) in saline solution was coinjected along with either Control or bPAC adenoviral vectors.

5,7-DHT treatments

To induce the depletion in the serotonergic system, rats were treated with a serotonergic neurotoxin: 5,7-dihydroxytryptamine hydrobromide (DHT; CDX-H0026-M010, Labclinics, Barcelona, Spain), 22 days after SCI (Fig. 6). Briefly, 20 μ L of 7.5 μ g/ml 5,7-DHT in 0.02% ascorbate saline solution was intraventricularly infused bilaterally (coordinates from bregma: AP: –0.8; ML: \pm 1.5; DV: –4.6; 10 μ L per side;

infusion rate: 1 μ l/min) both to bPAC (bPAC DHT) and control (control DHT) rats. The accessibility to the injection area required the removal of the optogenetic device. Injured sham controls (DHT-) were likewise injected with 0.02% ascorbate saline solution. The noradrenergic system was protected by intraperitoneal premedication (25 mg/kg) with desipramine hydrochloride (D3900, Merk Millipore Massachusetts, USA) 30 min before 5,7-DHT injections⁸⁹.

Statistics & reproducibility

Sample size determination: Sample sizes for the in vivo experiments were determined based on our previous experience and tailored to specific experimental needs. The following criteria were used: 1) For in vivo experiments involving functional testing, we selected larger sample sizes ($n = 9$ animals/group) were used to account for inherent variability of behavioral testing. 2) For histological analysis, group sizes ranged from $n = 3$ to 7 animals, as indicated in the manuscript for each experiment. 3) For in vitro experiments, for cAMP determinations we conducted three independent experiments derived from independent primary cultures, each with two technical replicates, while for Calcium live assays responses were recorded from individual neurons in two independent experiments. 4) for HPLC determination $n = 4$ animals considering the sensitivity of the technique, deemed sufficient given the method's sensitivity.

Data exclusion criteria. Data exclusions were performed according to the corresponding test of outlier detection as indicated for each case along the manuscript. Additionally, one animal was excluded after post-mortem evaluation of the injury size (calculated as the area negative for GFAP staining) because its injury area was 84.7% smaller than the average.

Independent reproducibility. Functional recovery in the animals was assessed through a long-term experiment lasting up to 35 days post-injury, $n = 9$ rats/group (as described in Fig. 3). Additional short-term experiments, including WGA and retrograde tracing studies, corroborated early-stage motor recovery differences (data not shown; data provided in source data Fig. 3C). Regarding the retrograde tracing experiment, a total of $n = 6$ animals per group were included, drawn from two independent experimental batches, which further supports the replicability of these results.

Randomization and blindness. In vivo experiments were randomized to assign animals to receive either bPAC or control viral vectors, minimizing potential confounds such as body weight. To ensure an even distribution of injury severity, all surgeries were performed by a single surgeon in a blinded and randomized manner. Post-mortem analysis of the injury area confirmed no significant differences between the control and bPAC groups, demonstrating the consistency of the injuries (Fig. 3B). Motor function evaluations were conducted in a blinded manner by two independent experimenters following the established guidelines for BBB motor scale evaluation.

Ethics approval

The maintenance and use of all animals were in accordance with guidelines established by the European Communities Council Directive (86/609/ECC) and the Spanish Royal Decree 53/2013. All experimental procedures were approved by the Animal Care and Use Committee of the Research Institute Prince Felipe (2021/VSC/PEA/0032).

Reporting summary

Further information on research design is available in the Nature Portfolio Reporting Summary linked to this article.

Data availability

Source data are provided with this paper. All used raw data generated in this study have been deposited in the Figshare database under

accession code <https://doi.org/10.6084/m9.figshare.28797458> Source data are provided with this paper.

References

- Arber, S. & Costa, R. M. J. S. Connecting neuronal circuits for movement. *Science*. **360**, 1403–1404 (2018).
- Dietz, V. J. N. R. N. Behavior of spinal neurons deprived of supraspinal input. *Nat. Rev. Neurol.* **6**, 167–174 (2010).
- de la Torre-Valdovinos, B., L. P. Osuna-Carrasco, and C. A. C. Ramos, *The Role of Supraspinal Structures for Recovery after SCI: From Motor Dysfunction to Mental Health, in Paraplegia*. (2021).
- Welniarz, Q., Dusart, I. & Roze, E. J. D. N. The corticospinal tract: evolution, development, and human disorders. *Dev. Neurobiol.* **77**, 810–829 (2017).
- Van Wittenberghe, IC. & Peterson, D. C. *Corticospinal Tract Lesion*. (Treasure Island (FL): StatPearls Publishing (NBK542201, 2023). Available from: <https://www.ncbi.nlm.nih.gov/books/NBK542201/>.
- Joosten, E. A. et al. Postnatal development of the ipsilateral corticospinal component in rat spinal cord: a light and electron microscopic anterograde HRP study. *J. Comp. Neurol.* **326**, 133–146 (1992).
- Isa, T., Tohyama, T. & Kinoshita, M. Phylogenetic view of the compensatory mechanisms in motor and sensory systems after neuronal injury. *Curr. Res. Neurobiol.* **3**, 100058 (2022).
- Liang, H. et al. Terminations of reticulospinal fibers originating from the gigantocellular reticular formation in the mouse spinal cord. *Brain Struct. Funct.* **221**, 1623–1633 (2016).
- Brownstone, R. M. & Chopek, J. W. J. F. I. N. C. Reticulospinal systems for tuning motor commands. *Front. neural circuits* **12**, 30 (2018).
- Mangold, S. A. and J. M. Das, *Neuroanatomy, Reticular Formation*, in (StatPearls Publishing, 2022).
- Asboth, L. et al. Cortico-reticulo-spinal circuit reorganization enables functional recovery after severe spinal cord contusion. *Nat. Neurosci.* **21**, 576–588 (2018).
- Antal, M. J. J.fH. Termination areas of corticobulbar and corticospinal fibres in the rat. *J. Hirnforsch.* **25**, 647–659 (1984).
- Keizer, K. & Kuypers, H. J. E. B. R. Distribution of corticospinal neurons with collaterals to the lower brain stem reticular formation in monkey (*Macaca fascicularis*). *Exp. Brain Res.* **74**, 311–318 (1989).
- Oudega, M. & Perez, M. A. J. T. J. O. P. Corticospinal reorganization after spinal cord injury. *J. Physiol.* **590**, 3647–3663 (2012).
- Hill, C. E., Beattie, M. S. & Bresnahan, J. C. J. E. N. Degeneration and sprouting of identified descending supraspinal axons after contusive spinal cord injury in the rat. *Exp Neurol.* **171**, 153–169 (2001).
- Álvarez, Z., et al., Bioactive scaffolds with enhanced supramolecular motion promote recovery from spinal cord injury. **374**, 848–856 (2021).
- Bradbury, E. J. et al. Chondroitinase ABC promotes functional recovery after spinal cord injury. *Nature* **416**, 636–640 (2002).
- Fischer, I., Dulin, J. N. & Lane, M. A. J. N. R. N. Transplanting neural progenitor cells to restore connectivity after spinal cord injury. *Nat. Rev. Neurosci.* **21**, 366–383 (2020).
- Lu, P. et al. Rehabilitation combined with neural progenitor cell grafts enables functional recovery in chronic spinal cord injury. *JCI Insight* **7**, e158000 (2022).
- Fink, K. L. & Cafferty, W. B. Reorganization of intact descending motor circuits to replace lost connections after injury. *Neurotherapeutics* **13**, 370–381 (2016).
- Bareyre, F. M. et al. The injured spinal cord spontaneously forms a new intraspinal circuit in adult rats. *Nat. Neurosci.* **7**, 269–277 (2004).
- Ishida, A. et al. Dynamic interaction between cortico-brainstem pathways during training-induced recovery in stroke model rats. *J. Neurosci.* **39**, 7306–7320 (2019).
- Kathe, C. et al. The neurons that restore walking after paralysis. *Nature* **611**, 540–547 (2022).

24. Lorach, H. et al. Walking naturally after spinal cord injury using a brain-spine interface. *Nature* **618**, 126–133 (2023).
25. Qiu, J. et al. Spinal axon regeneration induced by elevation of cyclic AMP. *Neuron* **34**, 895–903 (2002).
26. Neumann, S. et al. Regeneration of sensory axons within the injured spinal cord induced by intraganglionic cAMP elevation. *Neuron* **34**, 885–893 (2002).
27. Pearse, D. D. et al. cAMP and Schwann cells promote axonal growth and functional recovery after spinal cord injury. *Nat. Med* **10**, 610–616 (2004).
28. Lindner, R. et al. Photoactivation mechanism of a bacterial light-regulated adenylyl cyclase. *J. Mol. Biol.* **429**, 1336–1351 (2017).
29. Xiao, Y., Tian, W. & Lopez-Schier, H. Optogenetic stimulation of neuronal repair. *Curr. Biol.* **25**, R1068–R1069 (2015).
30. Stierl, M. et al. Light modulation of cellular cAMP by a small bacterial photoactivated adenylyl cyclase, bPAC, of the soil bacterium *Beggiatoa*. *J. Biol. Chem.* **286**, 1181–1188 (2011).
31. Halls, M. L. & Cooper, D. M. Regulation by Ca²⁺-signaling pathways of adenylyl cyclases. *Cold Spring Harb. Perspect. Biol.* **3**, a004143–a004143 (2011).
32. Zaccolo, M. & Pozzan, T. J. T. I. N. cAMP and Ca²⁺ interplay: a matter of oscillation patterns. *Trends Neurosci.* **26**, 53–55 (2003).
33. Hagiwara, M. et al. Gene expression and CREB phosphorylation induced by cAMP and Ca²⁺ in neuronal cells. *Adv. Pharmacol. (San Diego, Calif.)* **36**, 277–285 (1996).
34. Kleis, P. et al. Long-term in vivo application of a potassium channel-based optogenetic silencer in the healthy and epileptic mouse hippocampus. *BMC Biol.* **20**, 18 (2022).
35. Chen, L. et al. Cell type-specific decrease of the intrinsic excitability of motor cortical pyramidal neurons in Parkinsonism. *J. Neurosci. : J. Soc. Neurosci.* **41**, 5553–5565 (2021).
36. Jo, Y. et al. Poly-dipeptides produced from C9orf72 hexanucleotide repeats cause selective motor neuron hyperexcitability in ALS. *Proc. Natl. Acad. Sci. USA* **119**, e2113813119 (2022).
37. Cummings, B. J. et al. Adaptation of a ladder beam walking task to assess locomotor recovery in mice following spinal cord injury. *Behavioural brain Res.* **177**, 232–241 (2007).
38. Ascona, M., et al., *A Deep Learning-based Approach For Unbiased Kinematic Analysis in CNS Injury*. (2024).
39. Yang, S., et al., PACmn for improved optogenetic control of intracellular cAMP. **19**, 1–17 (2021).
40. Brösamle, C. & Schwab, M. E. Cells of origin, course, and termination patterns of the ventral, uncrossed component of the mature rat corticospinal tract. *J. Comp. Neurol.* **386**, 293–303 (1997).
41. Winter, C. C. et al. A transcriptomic taxonomy of mouse brain-wide spinal projecting neurons. *Nature* **624**, 403–414 (2023).
42. Nudo, R. J. & Masterton, R. B. Descending pathways to the spinal cord: a comparative study of 22 mammals. *J. Comp. Neurol.* **277**, 53–79 (1988).
43. Sengul, G. and C. Watson, Ascending and descending pathways in the spinal cord, in *The rat nervous system*. 115–130 Elsevier (2015).
44. Basile, G. A. et al. Red nucleus structure and function: from anatomy to clinical neuroscience. *Brain Struct. Funct.* **226**, 69–91 (2021).
45. Perreault, M.-C. & Giorgi, A. J. C. O. I. P. Diversity of reticulospinal systems in mammals. *Curr. Opin. Physiol.* **8**, 161–169 (2019).
46. Mullner, A. et al. Lamina-specific restoration of serotonergic projections after Nogo-A antibody treatment of spinal cord injury in rats. *Eur. J. Neurosci.* **27**, 326–333 (2008).
47. Zagon, A. & Bacon, S. J. E. J. oN. Evidence of a monosynaptic pathway between cells of the ventromedial medulla and the motoneuron pool of the thoracic spinal cord in rat: electron microscopic analysis of synaptic contacts. *Eur. J. Neurosci.* **3**, 55–65 (1991).
48. Jones S.L., & Light A. R. Termination of patterns of serotonergic medullary raphe-spinal fibers in the rat lumbar spinal cord: an anterograde immunohistochemical study. **297**, 267–282 (1990).
49. Alstermark, B., Kümmel, H. & Tantisira, B. Monosynaptic raphespinal and reticulospinal projection to forelimb motoneurons in cats. *Neurosci. Lett.* **74**, 286–290 (1987).
50. Perrier, J.-F. et al. Modulation of the intrinsic properties of motoneurons by serotonin. *Curr. Pharm. Des.* **19**, 4371–4384 (2013).
51. Levy, S. L. et al., Wheat germ agglutinin (WGA) tracing: a classic approach for unraveling neural circuitry. 51–66 (2015).
52. Choi, S., Jonak, E. & Fernstrom, J. D. J. B. R. Serotonin reuptake inhibitors do not prevent 5, 7-dihydroxytryptamine-induced depletion of serotonin in rat brain. *Brain Res.* **1007**, 19–28 (2004).
53. Ruschel, J. et al. Axonal regeneration. systemic administration of epothilone B promotes axon regeneration after spinal cord injury. *Science* **348**, 347–352 (2015).
54. Leibinger, M. et al. Transneuronal delivery of hyper-interleukin-6 enables functional recovery after severe spinal cord injury in mice. *Nat. Commun.* **12**, 391 (2021).
55. Anderson, M. A. et al. Natural and targeted circuit reorganization after spinal cord injury. *Nat. Neurosci.* **25**, 1584–1596 (2022).
56. Lynskey, J. V., Belanger, A. & Jung, R. Activity-dependent plasticity in spinal cord injury. *J. Rehabil. Res. Dev.* **45**, 229–240 (2008).
57. Nakagawa, H. et al. Reorganization of corticospinal tract fibers after spinal cord injury in adult macaques. *Sci. Rep.* **5**, 11986 (2015).
58. Gascon, S., Ortega, F. & Gotz, M. Transient CREB-mediated transcription is key in direct neuronal reprogramming. *Neurogenesis (Austin)* **4**, e1285383 (2017).
59. Caracciolo, L. et al. CREB controls cortical circuit plasticity and functional recovery after stroke. *Nat. Commun.* **9**, 2250 (2018).
60. Kadoya, K. et al. Spinal cord reconstitution with homologous neural grafts enables robust corticospinal regeneration. *Nat. Med.* **22**, 479–487 (2016).
61. Kim, J. E. et al. Nogo-66 receptor prevents raphespinal and rubrospinal axon regeneration and limits functional recovery from spinal cord injury. *Neuron* **44**, 439–451 (2004).
62. Courtine, G. et al. Transformation of nonfunctional spinal circuits into functional states after the loss of brain input. *Nat. Neurosci.* **12**, 1333–1342 (2009).
63. Liu, K. et al. PTEN deletion enhances the regenerative ability of adult corticospinal neurons. *Nat. Neurosci.* **13**, 1075–1081 (2010).
64. Pun, R. Y. et al. Excessive activation of mTOR in postnatally generated granule cells is sufficient to cause epilepsy. *Neuron* **75**, 1022–1034 (2012).
65. Golowasch, J. Neuromodulation of central pattern generators and its role in the functional recovery of central pattern generator activity. *J. Neurophysiol.* **122**, 300–315 (2019).
66. Pilyavskii, A. J. N., Corticofugal influences on reticulospinal neurons of the gigantocellular nucleus in cats. **8**, 192–199 (1976).
67. Del Cerro, P., Rodriguez-De-Lope, A. & Collazos-Castro, J. E. The cortical motor system in the domestic pig: origin and termination of the corticospinal tract and cortico-brainstem projections. *Front Neuroanat.* **15**, 748050 (2021).
68. Fisher, K. M. et al. Extensive Cortical Convergence to Primate Reticulospinal Pathways. *J. Neurosci.* **41**, 1005–1018 (2021).
69. Nathan, P., Smith, M. & Deacon, P. J. B. Vestibulospinal, reticulospinal and descending propriospinal nerve fibres in man. *Brain : a J. Neurol.* **119**, 1809–1833 (1996).
70. Perrin, F. E. et al. Anatomical study of serotonergic innervation and 5-HT(1A) receptor in the human spinal cord. *Cell Death Dis.* **2**, e218–e218 (2011).
71. Monreal-Trigo, J. et al. Optogenetic stimulation array for confocal microscopy fast transient monitoring. *IEEE Trans. Biomed. circuits Syst.* **16**, 1397–1405 (2022).
72. Joshi, A. et al. Handling considerations for the mass spectrometry of reactive organometallic compounds. *J. mass Spectrom. : JMS* **57**, e4807 (2022).

73. Xi, P., Liu, Y. & Ren, Q. *Scanning And Image Reconstruction Techniques In Confocal Laser Scanning Microscopy*, in *Laser Scanning, Theory and Applications*. (2011).
74. Walker, C. L. et al. Functional and histological gender comparison of age-matched rats after moderate thoracic contusive spinal cord injury. *J. neurotrauma* **36**, 1974–1984 (2019).
75. Watakabe, A. et al. Comparative analyses of adeno-associated viral vector serotypes 1, 2, 5, 8 and 9 in marmoset, mouse and macaque cerebral cortex. *Neurosci. Res.* **93**, 144–157 (2015).
76. Chen, M. et al. Corticospinal circuit neuroplasticity may involve silent synapses: Implications for functional recovery facilitated by neuromodulation after spinal cord injury. *IBRO Neurosci. Rep.* **14**, 185–194 (2023).
77. Basso, D. M., Beattie, M. S. & Bresnahan, J. C. J. J. O. N. A sensitive and reliable locomotor rating scale for open field testing in rats. *J. neurotrauma* **12**, 1–21 (1995).
78. Metz, G. A. & Whishaw, I. Q. J. J. O. N. M. Cortical and subcortical lesions impair skilled walking in the ladder rung walking test. *J. Neurosci. Methods* **115**, 169–179 (2002).
79. Allen, J. W., Yaksh, L. T. & protocols. Assessment of acute thermal nociception in laboratory animals. **99**, 11–23 (2004).
80. Gijlswijk, R. P. V. et al. Fluorochrome-labeled tyramides: use in immunocytochemistry and fluorescence in situ hybridization. *J. Histochem. Cytochem. J. Histochem. Soc.* **45**, 375–382 (1997).
81. Wang, L.-S. et al. LC-MS/MS-based quantification of tryptophan metabolites and neurotransmitters in the serum and brain of mice. *J. Chromatogr. B, Anal. Technol. Biomed. life Sci.* **1112**, 24–32 (2019).
82. Oeckl, P. & Ferger, B. J. J. O. N. M. Simultaneous LC–MS/MS analysis of the biomarkers cAMP and cGMP in plasma, CSF and brain tissue. *J. Neurosci. Methods* **203**, 338–343 (2012).
83. Morton, R. A., Y. Yanagawa, and C. F. J. E. Valenzuela, Electro-physiological assessment of serotonin and GABA neuron function in the dorsal raphe during the third trimester equivalent developmental period in mice, *eNeuro*. **2**, <https://doi.org/10.1523/ENEURO.0079-15.2015> (2015).
84. Andrade-Talavera, Y. et al. Ablation of p75NTR signaling strengthens gamma–theta rhythm interaction and counteracts A β -induced degradation of neuronal dynamics in mouse hippocampus in vitro. *Transl. psychiatry* **11**, 212 (2021).
85. Pérez-Rodríguez, M. et al. Adenosine receptor-mediated developmental loss of spike timing-dependent depression in the hippocampus. *Cereb. Cortex (N. Y., N. Y. : 1991)* **29**, 3266–3281 (2019).
86. Andrade-Talavera, Y. et al. Pre-synaptic kainate receptor-mediated facilitation of glutamate release involves PKA and Ca²⁺-calmodulin at thalamocortical synapses. *J. Neurochem.* **126**, 565–578 (2013).
87. Lyon, L. et al. Hippocampal mossy fiber long-term depression in Grm2/3 double knockout mice. *Synap. (N. Y., N. Y.)* **65**, 945–954 (2011).
88. Levy, S. L. et al. WGA-alexa conjugates for axonal tracing. *Curr. Protoc. Neurosci.* **79**, 1 28 1–1 28 24 (2017).
89. Bjömorklnd, A., H. Baumgarten, and A. J. J. O. N. Rensch, 5, 7-Dihydroxytryptamine: improvement of its selectivity for serotonin neurons in the CNS by pretreatment with desipramine. **24**, 833–835 (1975).

Acknowledgements

The publication of the present research is part of the project PID2021-124359OB-100 funded by MICIU/AEI /10.13039/501100011033 and by ERDF, UE (to VMM). This project has also received funding from the European Union's Horizon 2020 research and innovation program under grant agreement No. 964562 ("RISEUP") and Future and Emerging Technologies (FET) (to VMM). The Generalitat Valenciana funded part of the equipment employed in this work and co-financed with ERDF funds (OP ERDF of Comunitat Valenciana 2014–2020) and the UE; Fondo Europeo de Desarrollo Regional (FEDER) included in the Programa

Operativo FEDER de la Comunidad Valenciana 2014–2020. BMR was supported by a grant from the Conselleria de Educació, Investigació, Cultura y Deporte de la Generalitat Valenciana, and the European Social Foundation ACIF/2019/120. DS is supported by the European Commission ("BrainPlay", project-ID. 810580, to D.S.), by the Einstein Foundation, and the German Research Foundation (Deutsche Forschungsgemeinschaft, DFG): Germany's Excellence Strategy-EXC 2049 (NeuroCure, project-ID. 390688087), SFB1315 ("Mechanisms and Disturbances in Memory Consolidation: From synapses to systems", project-ID. 327654276). BRR is supported by the DFG: SFB1315 ("Mechanisms and Disturbances in Memory Consolidation: From synapses to systems", project-ID. 327654276). YAT was supported by a Marie Skłodowska-Curie Postdoctoral Fellowship under the Horizon Europe programme (GA.101061171). The authors also thank Dr Xavier Navarro Acebes, Pietro Fazzari, Juan Aguilar and Maria del Mar Sánchez for their scientific discussion and suggestions, and Stuart P. Atkinson for English editing and critical review of the manuscript.

Author contributions

Conceptualization, B.M.R., V.M.M. and E.G.; Methodology, B.M.R., V.M.M., E.G., E.L., A.A., G.P., M.P., S.M.P., Y.A.T., J.P.M., S.H., B.R., A.M., V.F., M.L.L.; Writing – Original Draft, B.M.R. and V.M.M.; Writing—Review & Editing, B.M.R., V.M.M., E.G., G.P., AM and BRR; Funding Acquisition, V.M.M., D.S.; Supervision, V.M.M. and E.G.

Competing interests

The authors declare no competing interests.

Additional information

Supplementary information The online version contains supplementary material available at <https://doi.org/10.1038/s41467-025-61018-3>.

Correspondence and requests for materials should be addressed to Beatriz Martínez-Rojas or Victoria Moreno-Manzano.

Peer review information *Nature Communications* thanks Francesco Fornai and the other anonymous reviewer(s) for their contribution to the peer review of this work. A peer review file is available.

Reprints and permissions information is available at <http://www.nature.com/reprints>

Publisher's note Springer Nature remains neutral with regard to jurisdictional claims in published maps and institutional affiliations.

Open Access This article is licensed under a Creative Commons Attribution-NonCommercial-NoDerivatives 4.0 International License, which permits any non-commercial use, sharing, distribution and reproduction in any medium or format, as long as you give appropriate credit to the original author(s) and the source, provide a link to the Creative Commons licence, and indicate if you modified the licensed material. You do not have permission under this licence to share adapted material derived from this article or parts of it. The images or other third party material in this article are included in the article's Creative Commons licence, unless indicated otherwise in a credit line to the material. If material is not included in the article's Creative Commons licence and your intended use is not permitted by statutory regulation or exceeds the permitted use, you will need to obtain permission directly from the copyright holder. To view a copy of this licence, visit <http://creativecommons.org/licenses/by-nc-nd/4.0/>.

© The Author(s) 2025